Vector-field guided constraint-following control for path following of uncertain mechanical systems

Hui Yin, *Member, IEEE*, Xiang Li, Yifan Liu, Weijia Yao, *Member, IEEE*

arXiv:2603.09472v1 [eess.SY] 10 Mar 2026

***Abstract*—This note proposes a general control approach, called vector-field guided constraint-following control, to solve the dynamics control problem of geometric path-following for a class of uncertain mechanical systems. More specifically, it operates at the dynamics level and can handle both fully-actuated and underactuated mechanical systems, heterogeneous (possibly fast) time-varying uncertainties with unknown bounds, and geometric desired paths that may be self-intersecting. Simulations are conducted to demonstrate the effectiveness of the approach.**

***Index Terms*—Geometric Path-following; Vector Field Guided Constraint-following; Uncertain Mechanical Systems.**

I. Introduction

Accurately following a geometric path is a fundamental task for robots, which requires a robot to converge to and move along the desired path with sufficient accuracy. This task does not require any temporal information on the desired path, thereby can alleviate performance limitations inherent to another important robot task—trajectory tracking [1]. Research on path-following algorithms has made remarkable progress in the past two decades [2]. Among them, those using a guiding vector field (GVF) have shown the ability to handle complex low- and high-dimensional geometric desired paths [3]–[5], and to achieve higher following accuracy using the least control effort compared to some other well-known algorithms [2].

However, currently the GVF builds its general theory based on the *kinematic* model rather than the *dynamic* model of a robot. The kinematic model only describes the relationship between the geometric states (e.g., displacement, velocity) of a robot and its internal actuators, without involving any forces/torques. Therefore, a GVF-based control generally provides displacement/velocity (rather than force/torque) guidance signal inputs to the robot, with the assumption that the robot-specific inner-loop dynamics control can accurately realize these inputs to support its effectiveness [2], [6], [7]. In other words, the current general theoretical results of GVF do not guarantee the convergence of robot dynamics to the desired path, which however is crucial for ensuring stable and accurate path-following. The integration of the dynamic model of a robot into the GVF-based path-following control design in a general theoretical framework remains challenging, especially when the dynamic model incorporates heterogeneous uncertainties, which is the common case in robot applications.

The constraint-following control (CFC) approach [8], [9], which uses the servo constraint [10]—mathematically a class of first-order ordinary differential equations (ODEs), to describe various control tasks (e.g., stabilization, trajectory-following), is specifically developed for the dynamics control of mechanical systems. More concretely, unlike the GVF, CFC builds its general theory by the *dynamic* model rather than the *kinematic* model of a mechanical system. It provides force/torque inputs to the system, guaranteeing the convergence of system dynamics to the servo constraint. Furthermore, it avoids linearizations, nonlinearity cancellations, and auxiliary variables (e.g., Lagrange multiplier) or pseudo variables (e.g., generalized speed). Without initial condition deviations and uncertainties, it is optimal for costs defined by either the integral or the instantaneous weighted norm of the control [11], [12]. However, regarding following tasks of robots, currently most CFC studies focus on trajectory-tracking rather than path-following. It is unclear yet how to generalize the CFC approach to solve geometric path-following problems. This note will, for the first time, reveal that the challenge arises from the servo constraint design to encode geometric desired paths.

Recognizing the importance of dynamics control in path-following, and noting the inherent connection between GVF and CFC, this note initiates a general approach that solves the dynamics control problem of geometric path-following for uncertain mechanical systems. The main contributions are twofold. First, a vector-field guided constraint-following control (VFCFC) framework is proposed, which operates at the dynamics level, and can deal with underactuated systems and self-intersecting desired paths. In the VFCFC, we meticulously design a vector-field guided constraint (VFC) to encode desired paths, by discovering the compatibility between the vector-field-guided ODE in GVF-based control and the constraint ODE in CFC. The relationship between VFC-

This work was supported by the National Natural Science Foundation of China under Grant 52475098.(*Corresponding author: Weijia Yao.*)

Hui Yin, Xiang Li are with the State Key Laboratory of Advanced Design and Manufacturing Technology for Vehicle, Hunan University, Changsha, 410082, China(e-mail: huiyin@hnu.edu.cn; lixiang2000@hnu.edu.cn).

Yifan Liu is with KUKA Robotics, Foshan, China, 528311, China(e-mail: lyf5400@hnu.edu.cn).

Weijia Yao is with the School of Artificial Intelligence and Robotics, Hunan University, Changsha, 410082, China(e-mail: wjyao@hnu.edu.cn).

following error and path-following error is rigorously analyzed, which theoretically supports VFC as a bridge connecting GVF and CFC that enables GVF to guide the system dynamics. Second, we introduce an adaptive robust method within the VFCFC for uncertainty suppression in path-following tasks for mechanical systems, where the uncertainty is considered in a very general form as detailed in Remark 1. In the method, we construct an adaptive law to online estimate the unknown uncertainty bound, and then invoke the estimated bound for uncertainty suppression (hence robust control). The contributions output two classes of VFCFCs , namely the nominal VFCFC guaranteeing vanishing path-following error for the nomnial system, and the adaptive robust VFCFC guaranteeing ultimately bounded path-following error for the uncertain system.

Notation: We denote by $\mathbb{R}$ and t the set of reals and the time, respectively. We use $\dot{x}(t)$ and $\ddot{x}(t)$ to respectively represent $\frac{\mathrm{d}}{\mathrm{d}t}x(t)$ and $\frac{\mathrm{d}^2}{\mathrm{d}t^2}x(t)$ for any C^2 function x of t. We denote by $\mathrm{dist}(p_0, \mathcal{S}) := \inf\{\|p_0 - p_\mathrm{s}\| : p_\mathrm{s} \in \mathcal{S}\}$ the distance between a point $p_0 \in \mathbb{R}^n$ and a nonempty set $\mathcal{S} \subseteq \mathbb{R}^n$, and denote by $\mathrm{dist}(\mathcal{S}_1, \mathcal{S}_2) := \inf\{\|p_{\mathrm{s}1} - p_{\mathrm{s}2}\| : p_{\mathrm{s}1} \in \mathcal{S}_1, p_{\mathrm{s}2} \in \mathcal{S}_2\}$ the distance between two nonempty sets $\mathcal{S}_1$ and $\mathcal{S}_2$. Consequently, the distance between a system trajectory $x(t) : [0, \infty) \to \mathbb{R}^n$ and a desired path $\mathcal{P} \subseteq \mathbb{R}^n$ is $\mathrm{dist}(x(t), \mathcal{P}) := \inf\{\|x(t) - p\| : p \in \mathcal{P}\}$, i.e., the path-following error at t.

II. Preliminaries and Problem Formulation

In this section, we first review some necessary preliminaries in Subsections II-A, II-B, and II-C. Then, the control problem is formulated in subsection II-D, which also provides a further explanation for the motivation of our solution strategy.

A. Uncertain mechanical systems

The dynamics of a controlled uncertain mechanical system can be generally described as

$$\begin{aligned} &M(q(t), \sigma(t), t)\ddot{q}(t) + C(q(t), \dot{q}(t), \sigma(t), t)\dot{q}(t) \\ &+ g(q(t), \sigma(t), t) = B(q(t), \sigma(t), t)\tau(t), \end{aligned} \tag{1}$$

where q, $\dot{q}$, $\ddot{q} \in \mathbb{R}^n$ denote the configuration, velocity, and acceleration vectors, respectively; $t \geq t_0 \geq 0$ with t_0 the initial time; $\sigma(t) \in \Sigma \subseteq \mathbb{R}^p$ denotes the time-varying uncertainty with Σ an unknown but compact set; The inertia matrix $M(q, \sigma, t) \in \mathbb{R}^{n\times n}$ is assumed to be positive definite and thus invertible, which holds for the vast majority of practical applications; $C(q, \dot{q}, \sigma, t)\dot{q}$, $g(q, \sigma, t) \in \mathbb{R}^n$ are the Coriolis/centrifugal and gravitational forces respectively, $B(q, \sigma, t) \in \mathbb{R}^{n\times m}$ is the input matrix and $\tau \in \mathbb{R}^m$ $(m \leq n)$ is the control force/torque. The functions M, C, g, B are all sufficiently smooth such that the existence and uniqueness of solutions to (1) is guaranteed for any given initial condition $(q(t_0), \dot{q}(t_0))$ [13, Theorem 3.1]. The system (1) can represent both fully-actuated (when $m = n$) and underactuated (when $m < n$) mechanical systems.

Remark 1. We only assume the uncertainty σ to be bounded, without assuming the bound Σ to be known. We also do not assume the time derivative of σ to be bounded, hence the uncertainty can be fast time-varying. As the considered system may be underactuated, mismatched uncertainty [14]—which enters the system through channels other than the control input—may be present in σ. Heterogeneous uncertainties can be cast into (1) by σ. For instance, parametric uncertainties can be directly described by σ, and unmodeled dynamics/external disturbances can be described by $C(q, \dot{q}, \sigma, t)\dot{q}$ or $g(q, \sigma, t)$. Therefore, (1) accommodates a broad class of uncertainties. ◀

B. Constraint-following control

Roughly speaking, the constraint-following control (CFC) is a solution to the so-called servo constraint problem of designing control forces that drive the state of a dynamical system to move in or toward a prespecified (servo) constraint manifold, i.e., constraint-following for short. To be precise, we first give a general definition of constraint following for dynamical systems. Then we particularize this definition for mechanical system (1), and subsequently gives the definition of CFC.

Definition 1 (constraint-following for dynamical systems)**.** Consider a dynamical system $\dot{x}(t) = F(x(t), t)$, $x \in \mathbb{R}^k$, with F piecewise-continuous in t and Lipschitz continuous in x. Given the initial condition $x(t_0) \in \mathbb{R}^k$, if there exists a constraint function $\beta : \mathbb{R}^k \times \mathbb{R}_{\geq t_0} \to \mathbb{R}^z$, such that $\|\beta(x(t), t)\| = 0$ for all $t \in \mathbb{R}_{\geq t_0}$, then the system trajectory $x(t)$ is said to *consistently satisfy* the constraint $\beta(x, t) = 0$. If $\lim_{t\to\infty} \|\beta(x(t), t)\| = 0$, or, for any $\epsilon > 0$, there exists a $T \in (0, \infty)$ such that $\|\beta(x(t), t)\| \leq \epsilon$ for all $t \geq T$, then $x(t)$ is said to *asymptotically follow* the constraint $\beta(x, t) = 0$. If $\|\beta(x(t), t)\|$ is uniformly ultimately bounded [13, Definition 4.6], then $x(t)$ is said to *approximately follow* the constraint $\beta(x, t) = 0$.

By Definition 1, if one replaces $x(t)$ with $(q(t), \dot{q}(t))$ of the mechanical system (1), and particularizes the constraint function β to a specific form, then the definition of constraint-following for mechanical systems in this study is given below.

Definition 2 (constraint-following for mechanical systems)**.** Given the initial condition $(q(t_0), \dot{q}(t_0)) \in \mathbb{R}^{2n}$ and the control input $\tau : \mathbb{R}_{\geq t_0} \to \mathbb{R}^m$ for the mechanical system (1), if the trajectory $(q(t), \dot{q}(t))$ of (1) satisfies

$$\sum_{i=1}^{n} a_{li}(q, t)\dot{q}_i - c_l(q, t) = 0, \qquad l = 1, \ldots, m \tag{2}$$

for all $t \geq t_0$, where $\dot{q}_i \in \mathbb{R}$ is the i-th entry of $\dot{q}$, and $a_{li}, c_l : \mathbb{R}^{n+1} \to \mathbb{R}$ are differentiable functions of q and t, then the trajectory $(q(t), \dot{q}(t))$ is said to *consistently satisfy* the constraint (2). Let $\beta_l(q, \dot{q}, t) := \sum_{i=1}^{n} a_{li}(q, t)\dot{q}_i - c_l(q, t)\,(l = 1, \cdots, m)$, $\beta := [\beta_1, \cdots, \beta_m]^\top$, if $\lim_{t\to\infty} \|\beta(q(t), \dot{q}(t), t))\| = 0$, then $(q(t), \dot{q}(t))$ is said to *asymptotically follow* the constraint (2). If $\|\beta(q(t), \dot{q}(t), t))\|$ is uniformly ultimately bounded, then $(q(t), \dot{q}(t))$ is said to *approximately follow* the constraint (2).

By Definition 2, the definition of CFC for mechanical systems is given below.

Definition 3 (CFC for mechanical systems)**.** Given the initial condition $(q(t_0), \dot{q}(t_0)) \in \mathbb{R}^{2n}$, if the trajectory $(q(t), \dot{q}(t))$ of the mechanical system (1) under a control input $\tau : \mathbb{R}_{\geq t_0} \to$

$\mathbb{R}^m$ *consistently satisfies* or *asymptotically/approximately follows* the constraint (2), then τ is a CFC for (1).

Rearranging (2) into the first-order matrix form yields:

$$A(q,t)\dot{q} = c(q,t), \tag{3}$$

where $A = [a_{li}]_{m\times n}$ and $c = [c_1, \dots, c_m]^\top$. Taking the time derivative of (3), we can obtain its second-order form as:

$$A(q,t)\ddot{q} = b(q,\dot{q},t), \tag{4}$$

where $b = \dot{c} - \dot{A}\dot{q}$ with $\dot{A} = [\dot{a}_{li}]_{m\times n}$ and $\dot{c} = [\dot{c}_1, \dots, \dot{c}_m]^\top$. By Definition 2 and (3), we have

$$\beta(q,\dot{q},t) = A(q,t)\dot{q} - c(q,t), \tag{5}$$

which can be interpreted as the *constraint-following error*. If $\beta(q(t),\dot{q}(t),t) = 0$, then the current states $(q(t),\dot{q}(t))$ satisfy the constraint (3). In view of (4), the time derivative of (5) is

$$\dot{\beta}(q,\dot{q},t) = A(q,t)\ddot{q} - b(q,\dot{q},t).$$

It has been demonstrated [8] that various control problems, including stabilization and trajectory-tracking, can be encoded by the proposed constraint form. However, it is unclear yet how to use the proposed constraint form to deal with the path-following problem in a general theoretical framework.

Assumption 1. For each $(q,\dot{q},t) \in \mathbb{R}^n \times \mathbb{R}^n \times \mathbb{R}$, there is at least one solution $\ddot{q} \in \mathbb{R}^n$ to the constraint (4).

Remark 2. Assumption 1 simply implies that in principle the designed constraint has to be feasible, so that the constraint-following task is possible. A necessary and sufficient condition to verify Assumption 1 is, the equation $A(q,t)A^+(q,t)b(q,\dot{q},t) = b(q,\dot{q},t)$ holds for all $(q,\dot{q},t) \in \mathbb{R}^n \times \mathbb{R}^n \times \mathbb{R}$, with the superscript "+" denoting the Moore-Penrose (MP) generalized inverse. This is an indispensable assumption to rule out impossible constraint-following tasks. ◀

C. Guiding vector field

This subsection first introduces the simple 2-D guiding vector fields (GVFs) to show the basic concept. Then the more abstract general case with higher dimensions is presented.

1) GVF in $\mathbb{R}^2$ for non-self-intersecting desired path: Suppose the desired path $\mathcal{P}$ is described by

$$\mathcal{P} = \{(q_1,q_2) \in \mathbb{R}^2 : \psi(q_1,q_2) = 0\},$$

where $\psi : \mathbb{R}^2 \to \mathbb{R}$ is twice continuously differentiable. If $\mathcal{P}$ is non-self-intersecting, then a valid GVF $\chi : \mathbb{R}^2 \to \mathbb{R}^2$ for $\mathcal{P}$ can be designed as [4], [6]:

$$\chi(q_1,q_2) = E\nabla\psi(q_1,q_2) - k\psi(q_1,q_2)\nabla\psi(q_1,q_2), \tag{6}$$

where $E = \begin{bmatrix} 0 & -1 \\ 1 & 0 \end{bmatrix}$, $k \in \mathbb{R}_+$ is a constant, $\nabla\psi(q_1,q_2)$ is the gradient of ψ. On the RHS (right-hand side) of (6), the first term is "tangential" to $\mathcal{P}$, called the propagation term and steering a system to traverse along $\mathcal{P}$. The second term is perpendicular to the first term, called the convergence term and steering a system to move closer to $\mathcal{P}$.

Even under the assumption that $\mathcal{P}$ is non-self-intersecting, there may be singularity points where $\chi(q_1,q_2) = 0$ in (6) resulting in the vanishing of guiding signals. For example, when $\mathcal{P}$ is a simple closed circle centered at the origin, the origin is a singular point. Therefore, the following will introduce the singularity-free GVF for the general case, where the desired path can be either simple closed or self-intersecting [15].

2) General singularity-free GVF: Suppose a physical desired path $\mathcal{P} \subseteq \mathbb{R}^m$ that may be simple closed or self-intersecting is described by the intersection of $(m-1)$ hypersurfaces

$$\mathcal{P} = \{\zeta := [q_1, \dots, q_m]^\top \in \mathbb{R}^m : \psi_i(\zeta) = 0, i = 1, \cdots, m-1\}, \tag{7}$$

which can be parameterized by

$$q_1 = f_1(w), \quad \dots, \quad q_m = f_m(w).$$

Here, ζ is the physical coordinate, $f_i \in C^2$, $i = 1, \cdots, m$, and $w \in \mathbb{R}$ is the parameter; furthermore, there exists a scalar $\epsilon > 0$ such that $f_i'(w) := \frac{\mathrm{d}f_i(w)}{\mathrm{d}w}$ satisfies $|f_i'(w)| \le \epsilon$.

Let $\phi_i(q_1, \dots, q_m, w) := q_i - f_i(w)$ $(i = 1, \cdots, m)$ and $\xi := [\zeta^\top, w]^\top$ with w being viewed as an additional virtual coordinate. Then we can obtain a higher dimensional desired path in the $(m+1)$-dimensional ξ-space as

$$\mathcal{P}^{hgh} = \{\xi \in \mathbb{R}^{m+1} : \phi_i(\xi) = 0, i = 1, \dots m\}.$$

Remark 3. Intuitively, the $(m+1)$-D path $\mathcal{P}^{hgh}$ is obtained by "cutting" and "stretching" the m-D path $\mathcal{P}$ along the virtual w-axis. Inversely speaking, the path $\mathcal{P}$ is the orthogonal projection of the path $\mathcal{P}^{hgh} \subseteq \mathbb{R}^{m+1}$ in the space $\mathbb{R}^m$ with the remaining w-axis as zero. We can also obtain that, for a virtual system trajectory $\xi(t)$ living in the same $(m+1)$-D space as $\mathcal{P}^{hgh}$, its orthogonal projection in the m-D space where $\mathcal{P}$ lives, is the physical system trajectory $\zeta(t)$. It has been shown in [15] that the path-following errors $\mathrm{dist}(\xi(t), \mathcal{P}^{hgh})$ and $\mathrm{dist}(\zeta(t), \mathcal{P})$ have the same convergence behaviour. Therefore, we can investigate $\mathrm{dist}(\zeta(t), \mathcal{P})$ by $\mathrm{dist}(\xi(t), \mathcal{P}^{hgh})$. ◀

The gradients of ϕ_i $(i = 1, \cdots, m)$ are $\nabla\phi_i = [0, \cdots, 1, \cdots, -f_i'(w)]^\top$, where "1" is the i-th element of $\nabla\phi_i$. Then by [15], the GVF for $\mathcal{P}^{hgh}$ is constructed as

$$\chi(\xi) = \begin{bmatrix} (-1)^m f_1'(w) - k_1\phi_1(\xi) \\ \vdots \\ (-1)^m f_m'(w) - k_m\phi_m(\xi) \\ (-1)^m + \sum_{i=1}^m k_i\phi_i(\xi)f_i'(w) \end{bmatrix} \in \mathbb{R}^{m+1}, \tag{8}$$

where $k_i > 0, i = 1, \cdots, m$, are constant gains. The first and second terms on the RHS of (8) are the propagation and converging terms, respectively, which are always linearly independent unless they all equal zero. Therefore, the last element of χ in (8) is always non-zero, and the GVF χ is singularity-free, i.e., $\chi(\xi) \neq 0$ for any $\xi \in \mathbb{R}^{m+1}$. This appealing property of χ is attributed to the introduction of the additional dimension w, and thus the assumption of no singular points that may limit the range of admissible desired paths becomes unnecessary. Therefore, this note will adopt only the singularity-free GVF, and all the results can also be applied to the general GVF in [4].

By the GVF χ, the trajectories of the following system:

$$\dot{\xi}(t) = \chi(\xi(t)) \tag{9}$$

will globally asymptotically converge to and move along the desired path without requiring the origin of the system to be stable (see [15, Theorem 2]). Therefore, if one can design a control to drive the trajectory of a mechanical system to satisfy (9), then the path-following task can be completed.

D. Problem formulation

1) Problem statement: Consider uncertain mechanical systems with dynamic model (1), the control problem is to design

a state feedback control τ that drives the system trajectories to follow the desired path $\mathcal{P} \subseteq \mathbb{R}^m$ defined like (7):

$$\mathcal{P} = \{q^{\mathrm{s}} \in \mathbb{R}^m : \psi_i(q^{\mathrm{s}}) = 0, i = 1, \cdots, m-1\}, \tag{10}$$

where $q^{\mathrm{s}} \in \mathbb{R}^m$ comprises some or all entries of $q \in \mathbb{R}^n$, not necessarily being $[q_1, \ldots, q_m]^\top$.

The proposed solution is motivated by a capability analysis of existing CFCs and GVF-based controls. This motivation will be further explained later. Because the GVF χ in (8) will be used, τ may draw values from the domains of both physical states $(q, \dot{q})$ and extended state w.

2) Motivated solution strategy: In the CFC approach, the constraint is specified as (3) to describe control tasks. Using (3), conventional methods reformulate desired path (10) into the following equivalent form: $\dot{\psi}(q^{\mathrm{s}}) + \Lambda\psi(q^{\mathrm{s}}) = 0$ with $\Lambda > 0$ a constant matrix. Such methods pose two issues. First, the resulting matrix A includes the derivative of $\psi(q^{\mathrm{s}})$ with respect to q^{s}. This indicates that A will be state-dependent once $\psi(q^{\mathrm{s}})$ is nonlinear in q^{s}, which may lead to the violation of Assumption 1 (as illustrated by an example in the simulation section). Second, the resulting CFC can only guarantee system trajectories to follow the above constraint to approach the desired path, but cannot guarantee system trajectories to move along the desired path.

In the GVF-based control approach, given the GVF (8), the remaining task is to design a control such that the dynamics of ξ associated with a mechanical system satisfies (9). However, current GVF-based control design approaches use kinematic models of robotic systems, assuming an effective system-specific inner-loop dynamics control, and cannot be directly applied to the dynamic model (1) of mechanical systems.

Comparing ODEs (3) and (9), we can find that (9) can be cast into the form of (3), with a constant (state-independent) matrix A. This implies a bridge between CFC and GVF. Given the complementary strengths and limitations of CFC and GVF in addressing path-following tasks, bridging them suggests a promising solution to the stated control problem. The realization of this idea represents the first contribution claimed in the introduction, which is detailed in subsequent sections.

III. Main results

A. Vector-field guided constraint

Regarding the GVF χ used in this study, i.e., (8), ξ includes a virtual position coordinate w, and (9) can be rewritten into two parts: one corresponding to $\dot{\zeta}$, and the other corresponding to $\dot{w}$. The part of $\dot{\zeta}$ is

$$\dot{\zeta}(t) = \chi^{\mathrm{s}}(\xi(t)), \tag{11}$$

where

$$\chi^{\mathrm{s}}(\xi) = \begin{bmatrix} (-1)^m f_1'(w) - k_1\phi_1(\xi) \\ \vdots \\ (-1)^m f_m'(w) - k_m\phi_m(\xi) \end{bmatrix} \in \mathbb{R}^m.$$

The part of $\dot{w}$ is

$$\dot{w} = (-1)^m + \sum_{i=1}^{m} k_i\phi_i(\xi) f_i'(w) \in \mathbb{R}. \tag{12}$$

As $q^{\mathrm{s}} \in \mathbb{R}^m$ consists of some (or all) entries of $q \in \mathbb{R}^n$ in (1), there exists a linear relation between q and q^{s}. Namely, there exists a constant matrix $A \in \mathbb{R}^{m\times n}$ of full row rank that can be constructed in a general way, such that $Aq = q^{\mathrm{s}}$. A method to construct A is presented as follows. Suppose that the vector $q^{\mathrm{s}} = [q_{s_1}, q_{s_2}, \cdots, q_{s_m}]^\top$, with $s_1 < s_2 < \cdots < s_m$ and $s_i \in \{1, 2, , \cdots, n\}, i = 1, \cdots, m$. Note that $q = [q_1, q_2, \cdots, q_n]^\top$. Then the element at the i-th row and j-th column in the $m \times n$ matrix A satisfying $Aq = q^{\mathrm{s}}$ is

$$a_{ij} = \begin{cases} 1, & \text{if } s_i = j, \\ 0, & \text{otherwise.} \end{cases}$$

Let $\zeta := q^{\mathrm{s}}$, then $\xi = (\zeta^\top, w)^\top$, and the part of $\dot{\zeta}$ (11) can be re-written as follows

$$\dot{\zeta}(t) = A\dot{q}(t) = \chi^{\mathrm{s}}(Aq(t), w(t)). \tag{13}$$

Comparing (3) and (13), one immediately obtains that (13) can be viewed as the constraint in the CFC framework. Namely, the CFC can be used to enable the trajectory $q(t)$ of uncertain mechanical system (1) to satisfy constraint (13) and eventually follow the desired path encoded in (13). As (13) is constructed based on the vector field, we call it the *vector-field guided constraint (VFC)*, and the resulting CFC is called the *vector-field guided constraint-following control (VFCFC)*. The second order form of (13) can be cast into (4) with A being the same as that in (13) and

$$b(q, \dot{q}, w) = \dot{\chi}^{\mathrm{s}}(q, w) \overset{(12)}{=} \frac{\partial \chi^{\mathrm{s}}(q, w)}{\partial q}\dot{q} + \frac{\partial \chi^{\mathrm{s}}(q, w)}{\partial w}\left[(-1)^m + \sum_{i=1}^{m} k_i\phi_i(\xi) f_i'(w)\right].$$

Remark 4. Note that the part of $\dot{w}$ (12) is not included in the VFC, since (12) is a designed virtual system which as an equation always holds for each real-time measurement of q. Nevertheless, (12) will serve as a virtual "adjoint system" governing the evolution of w to "shape" the VFC (13) dynamically for the control design. Concretely, for any given initial value $w(t_0)$ and each real-time measured q, the control algorithm simply needs to substitute q into (12) and solve it to obtain w. The resulting w can then be used in the VFC (13) as the desired system motion being the control goal. In a word, to fulfill the path-following task, we only need to design a control to drive the motion of system (1) to follow (13) with a virtual "adjoint system" (12) governing w, which is similar to the adaptive law governing adaptive parameters in adaptive controls [16]. ◀

Remark 5. It is worth emphasizing that the matrix A of the VFC is constant and of full row rank, which brings essential benefits to the CFC design for path-following. The most salient one is, with such a matrix A, the fundamental Assumption 1 to rule out impossible constraint-following tasks is always satisfied. While in conventional CFC design, Assumption 1 has to be cautiously verified. Furthermore, the matrix A is generally involved in some other assumptions within the CFC framework, e.g., [9] assuming A to be of full row rank. A constant A of full row rank, instead of a state-dependent A, will greatly ease the restrictions arising from these assumptions. ◀

B. Error analysis

In this subsection, error analysis will be implemented to assure the effectiveness of VFC for encoding the path-following task. From the above discussion, we can find that there are three error signals of the actual system trajectory.

1. The first error signal is the *path-following error*:

$$\mathrm{dist}(\xi(t), \mathcal{P}^{hgh}) = \inf\{\|\xi(t) - p\| : p \in \mathcal{P}^{hgh}\}.$$

Rendering $\mathrm{dist}(\xi(t), \mathcal{P}^{hgh})$ to converge to 0 or to be (ultimately) bounded as $t \to \infty$ is the ultimate control goal. However, $\mathrm{dist}(\xi(t), \mathcal{P}^{hgh})$ is generally computationally complicated.

2. The second error signal is the *path-function error*:

$$\|\phi(\xi)\| = \|[\phi_1(\xi), \phi_2(\xi), \cdots, \phi_{m-1}(\xi)]^\top\|,$$

which is more straightforward for computation. It is introduced to "represent" the path-following error $\mathrm{dist}(\xi, \mathcal{P}^{hgh})$, in the sense that $\|\phi(\xi)\|$ converging to zero implies $\mathrm{dist}(\xi, \mathcal{P}^{hgh})$ converging to zero along a trajectory $\xi(t)$, and the boundedness of $\|\phi(\xi)\|$ implies the boundedness of $\mathrm{dist}(\xi, \mathcal{P}^{hgh})$ along a trajectory $\xi(t)$. This is guaranteed under two mild assumptions (i.e., Assumptions 2 and 3) that will be imposed later to guarantee the consistency of convergence behaviors between the path-following error $\mathrm{dist}(\xi, \mathcal{P}^{hgh})$ and the path-function error $\|\phi(\xi)\|$, so that we can use $\|\phi(\xi)\|$ to "represent" the path-following error.

3. The third error signal is the *VFC-following error*:

$$\beta(q, \dot{q}, w) = A\dot{q} - \chi^{\mathrm{s}}(Aq, w),$$

which can be directly used to indicate the satisfaction of VFC (13). We will show in the sequel that the convergence behavior of $\|\beta\|$ aligns with that of $\|\phi\|$. Therefore, the path-following control design task can be fulfilled by analyzing $\|\beta\|$, as long as certain consistency of convergence behaviors between the path-following error $\mathrm{dist}(\xi, \mathcal{P}^{hgh})$ and the path-function error $\|\phi(\xi)\|$ is guaranteed.

The VFC-following error β indicates the distance between $\dot{\zeta}$ and χ^{s}, which affects the satisfaction of (13). Furthermore, as the part of $\dot{w}$ (12) always holds, it does not bring any errors. Consequently, we can obtain the disturbed system of (9) as

$$\dot{\xi}(t) = \chi(\xi(t)) + d(t)$$

with $d(t) = [\beta^\top(q(t), \dot{q}(t), w(t)), 0]^\top \in \mathbb{R}^{m+1}$ being the disturbance. Then the governing equation of ϕ is

$$\dot{\phi}(\xi(t)) = N^\top(\xi(t))(\chi(\xi(t)) + d(t)) \tag{14}$$

with $N(\xi) = [\nabla\phi_1(\xi), \nabla\phi_2(\xi), \cdots, \nabla\phi_m(\xi)] \in \mathbb{R}^{(m+1)\times m}$. With the governing equation (14) of path-function error ϕ, the following subsections will demonstrate the feasibility of using the convergence behavior of VFC-following error $\|\beta\|$ to indicate that of path-following error $\mathrm{dist}(\xi, \mathcal{P}^{hgh})$. The demonstration is carried out considering two different cases: vanishing d and non-vanishing but bounded d.

1) Vanishing disturbance:

Assumption 2. For any positive scalar constant ϵ, it holds that

$$\inf\{\|\phi(\xi(t))\| : \mathrm{dist}(\xi(t), \mathcal{P}^{hgh}) \geq \epsilon\} > 0.$$

Remark 6. Assumption 2 implies that along any continuous trajectory $\xi(t) : [0, \infty) \to \mathbb{R}^{m+1}$, we have $\|\phi(\xi(t))\| \to 0 \implies \mathrm{dist}(\xi(t), \mathcal{P}^{hgh}) \to 0$ as $t \to \infty$. Namely, once we know that $\|\phi\|$ vanishes along a trajectory, then the distance from the trajectory to the desired path also vanishes. This assumption enables us to use $\|\phi\|$ to indicate the convergence behaviour of $\mathrm{dist}(\xi, \mathcal{P}^{hgh})$ when $\|\phi\|$ vanishes, which will serve as a base for the following proposition to show that vanishing $\|\beta\|$ or $\|d\|$ leads to vanishing $\mathrm{dist}(\xi, \mathcal{P}^{hgh})$. ◀

Proposition 1. *Under Assumption 2, the path-following error* $\mathrm{dist}(\xi(t), \mathcal{P}^{hgh})$ *will converge to* 0 *if* $\|\beta(q(t), \dot{q}(t), w(t))\| = \|d(t)\| \to 0$ *as* $t \to \infty$.

Proof. By [4, Theorem 3], the governing equation (14) of the path-function error $\phi(\xi(t))$ is locally input-to-state stable with $d(t)$ being the input, which implies that the error satisfies $\|\phi(\xi(t))\| \leq \eta(\|\phi(\xi(t_0))\|, t) + \varrho(\sup_{r\in[t_0,t)} \|d(r)\|)$ for a class $\mathcal{KL}$ function η and a class $\mathcal{K}$ function ϱ. Since $\|d\| \equiv \|\beta\|$ and $\|\beta(q(t), \dot{q}(t), w(t))\| \to 0$ as $t \to \infty$, $\|\phi(\xi(t))\| \to 0$ as $t \to \infty$. By Assumption 2, we have that $\mathrm{dist}(\xi(t), \mathcal{P}^{hgh})$ converges to 0 as $t \to \infty$. ■

2) Non-vanishing but bounded disturbance:

Assumption 3. It holds that $\|\phi(\xi)\| \to \infty$ as $\mathrm{dist}(\xi, \mathcal{P}^{hgh}) \to \infty$ for $\xi \in \mathbb{R}^{m+1}$.

Remark 7. Technically, Assumption 3 implies that for any $\epsilon > 0$, there exists $\epsilon_0 > 0$, such that if $\mathrm{dist}(\xi, \mathcal{P}^{hgh}) > \epsilon_0$, then $\|\phi(\xi)\| > \epsilon$. In other words, we have $\{\xi : \|\phi(\xi)\| \leq \epsilon\} \subseteq \{\xi : \mathrm{dist}(\xi, \mathcal{P}^{hgh}) \leq \epsilon_0\}$, indicating that the distance $\mathrm{dist}(\xi(t), \mathcal{P}^{hgh})$ is bounded if $\|\phi(\xi(t))\|$ is bounded along any continuous trajectory $\xi(t)$. This enables us to use $\|\phi(\xi)\|$ to investigate the convergence behaviour of $\mathrm{dist}(\xi, \mathcal{P}^{hgh})$ when $\|\phi(\xi)\|$ is bounded, which will serve as a base for the following proposition to show that bounded $\|\beta\|$ or $\|d\|$ leads to bounded $\mathrm{dist}(\xi, \mathcal{P}^{hgh})$. ◀

Proposition 2. *Under Assumption 3, the path-following error* $\mathrm{dist}(\xi(t), \mathcal{P}^{hgh})$ *is uniformly ultimately bounded if* $\|\beta(q(t), \dot{q}(t), w(t))\| = \|d(t)\|$ *is uniformly bounded.*

Proof. As $\|d\| \equiv \|\beta\|$, we have $\sup_{r\in[t_0,t)} \|d(r)\| = \sup_{r\in[t_0,t)} \|\beta(q(r), \dot{q}(r), w(r))\|$. From the proof of Proposition 1, the path-function error $\|\phi(\xi(t))\|$ is uniformly ultimately bounded by a $\mathcal{K}$-class function of $\sup_{r\in[t_0,t)} \|\beta(q(r), \dot{q}(r), w(r))\|$, i.e., $\varrho(\sup_{r\in[t_0,t)} \|\beta(q(r), \dot{q}(r), w(r))\|)$, since the governing equation (14) of $\phi(\xi(t))$ is locally input-to-state stable with $d(t)$ being the input. Applying Assumption 3, we have that $\mathrm{dist}(\xi(t), \mathcal{P}^{hgh})$ is uniformly ultimately bounded. ■

From Propositions 1 and 2, it follows that if the control law designed for (1) ensures that the VFC-following error $\|\beta(q(t), \dot{q}(t), w(t))\|$ converges to 0 or remains uniformly bounded as $t \to \infty$, then the path-following error $\mathrm{dist}(\xi, \mathcal{P}^{hgh})$ exhibits consistent convergence behaviour, provided that mild assumptions are satisfied. Therefore, the path-following task associated with the desired path $\mathcal{P}$ in (10) can be transformed to the constraint-following task associated with the VFC (13), which will be fulfilled in the following subsection.

Based on the above results, the control design for the path-following problem of the mechanical system (1) proceeds in two steps. First, neglecting the uncertainty, a class of nominal

path-following controls is designed. Second, considering the uncertainty, a class of adaptive robust path-following controls is designed based on the nominal control.

C. Nominal path-following control

The nominal system of (1) can be described as

$$\bar{M}(q(t),t)\ddot{q}(t)+\bar{C}(q(t),\dot{q}(t),t)\dot{q}(t) \\ +\bar{g}(q(t),t)=\bar{B}(q(t),t)\tau(t). \tag{15}$$

In this study, the nominal and uncertain portions of a system matrix $(\cdot)$ are denoted by $\bar{(\cdot)}$ and $\Delta(\cdot)$ respectively, hence $(\cdot)=\bar{(\cdot)}+\Delta(\cdot)$. For example, $\bar{M}$ represents the nominal portion of M, which is also considered to be positive definite. The nominal path-following control that steers the nominal system (15) to follow $\mathcal{P}$ is designed under the following assumption.

Assumption 4. For any given constant matrix $P\in\mathbb{R}^{m\times m}$, $P>0$, there exists a positive constant $\underline{\lambda}>0$ such that $\lambda_m(PA\bar{M}^{-1}(q,t)\bar{B}(q,t)(A\bar{M}^{-1}(q,t)\bar{B}(q,t))^\top P)\geq\underline{\lambda}$ for all $(q,t)\in\mathbb{R}^n\times\mathbb{R}_{\geq 0}$, where $\lambda_m(\cdot)$ denotes the minimal eigenvalue of a matrix.

Remark 8. Note $PA\bar{M}^{-1}(q,t)\bar{B}(q,t)(A\bar{M}^{-1}(q,t)\bar{B}(q,t))^\top P$ is positive semi-definite for all $(q,t)\in\mathbb{R}^n\times\mathbb{R}_{\geq 0}$, i.e., all of its eigenvalues are non-negative. Assumption 4 simply requires that the minimum eigenvalue remain bounded away from zero, i.e., it does not approach zero infinitesimally. Another implication of Assumption 4 is that the matrix $A\bar{M}^{-1}(q,t)\bar{B}(q,t)$ is invertible for all $(q,t)\in\mathbb{R}^n\times\mathbb{R}$. A similar assumption is frequently adopted in existing CFC design studies [17], [18]. This assumption excludes tasks where the matrix A results in a non-invertible $A\bar{M}^{-1}(q,t)\bar{B}(q,t)$ for some $(q,t)\in\mathbb{R}^n\times\mathbb{R}$, as its inverse is required in the control design. However, the distinction lies in the fact that Assumption 4 in this study uses a constant A that is of full row rank, whereas the corresponding assumption in existing CFC studies involves an A that depends on (q,t). This difference stems from the proposed VFC, which greatly relaxes the restrictions arising from this assumption. ◀

The nominal path-following control is proposed as

$$\tau(t)=p_1(q(t),\dot{q}(t),w(t),t)+p_2(q(t),\dot{q}(t),w(t),t), \tag{16}$$

with

$$p_1(q,\dot{q},w,t)=(A\bar{M}^{-1}(q,t)\bar{B}(q,t))^{-1}[b(q,\dot{q},w) \\ +A\bar{M}^{-1}(q,t)(\bar{C}(q,\dot{q},t)\dot{q}+\bar{g}(q,t))], \tag{17}$$

$$p_2(q,\dot{q},w,t)=-\kappa(A\bar{M}^{-1}(q,t)\bar{B}(q,t))^\top P\beta(q,\dot{q},w),$$

and $\beta=A\dot{q}-\chi^{\mathrm{s}}$, $\kappa\in\mathbb{R}_+$ is a gain parameter.

Theorem 1 (Vanishing of nominal system)**.** *Under Assumptions 2 and 4, the path-following control (16) drives the trajectory of the nominal mechanical system (15) to converge to the desired path (10), i.e., the path-following error satisfies that* $\mathrm{dist}(\zeta(t),\mathcal{P})\to 0$ *as* $t\to\infty$.

Proof. By the results in [17, Theorem 2], it follows that $\beta(q(t),\dot{q}(t),w(t))=A\dot{q}(t)-\chi^{\mathrm{s}}(Aq(t),w(t))$ exponentially converges to 0 as $t\to\infty$. Namely, the trajectory of the nominal mechanical system (15) asymptotically follows the constraint (13) (c.f., Definition 2). Then by Proposition 1, since the VFC-following error converges to 0 as $t\to\infty$, the path-following error $\mathrm{dist}(\xi(t),\mathcal{P}^{hgh})$ converges to 0 as $t\to\infty$, and thus by Remark 3, we have $\mathrm{dist}(\zeta(t),\mathcal{P})\to 0$ as $t\to\infty$. □

D. Adaptive robust path-following control

To robustly achieve path-following for the uncertain system (1) with the desired path (10), this section designs an adaptive robust action p_3 added to the nominal control (16) to suppress uncertainty, resulting in a class of adaptive robust path-following controls. Due to the uncertainties, vanishing path-following error is not always possible, while the best achievable performance is typically the boundedness of the path-following error, which is the objective of the p_3 design.

To handle the mismatched uncertainty, we perform the following uncertainty decompositions. Let $H:=\bar{M}M^{-1}-I$, which is employed to represent the uncertainty in M. Let

$$H(q,\sigma,t)=\bar{B}(q,t)\check{H}(q,\sigma,t)+\tilde{H}(q,\sigma,t). \tag{18}$$

This is to divide H into two portions based on $\bar{B}$, i.e., the matched uncertainty $\bar{B}\check{H}$ and the mismatched uncertainty $\tilde{H}$, which lies within and outside the range space of $\bar{B}$, respectively. Throughout the paper, we use $\check{(\cdot)}$ and $\tilde{(\cdot)}$ to respectively denote matched and mismatched portions. There are infinite choices for the particular expressions of $\check{H}$ and $\check{H}$. For example, one may choose any $\check{H}$ and let $\tilde{H}:=H-\bar{B}\check{H}$. However, we meticulously chose $\check{H}$ and then obtain $\tilde{H}$ by (18) as follows

$$\check{H}=(A\bar{M}^{-1}\bar{B})^{-1}A\bar{M}^{-1}H, \\ \tilde{H}=H-\bar{B}(A\bar{M}^{-1}\bar{B})^{-1}A\bar{M}^{-1}H, \tag{19}$$

where recall that $A\bar{M}^{-1}\bar{B}$ is invertible by Assumption 4. Similar to (18), other uncertain system matrices, ΔC, Δg, and ΔB, can also be decomposed based on the nominal matrix $\bar{B}$. The detailed expressions for these decompositions are omitted here for simplicity. From (19), we obtain the following identity regarding the mismatched uncertainty $\tilde{H}$

$$A\bar{M}^{-1}\tilde{H}=A\bar{M}^{-1}[H-\bar{B}(A\bar{M}^{-1}\bar{B})^{-1}A\bar{M}^{-1}H]\equiv 0.$$

Similarly, it can be shown that the mismatched uncertainties of other uncertain system matrices satisfy analogous identities, i.e., $A\bar{M}^{-1}\tilde{(\cdot)}\equiv 0$, where $(\cdot)$ represents C, g or B.

Assumption 5. There exists a (possibly unknown) constant $\rho_W>-1$ such that for all $(q,t)\in\mathbb{R}^n\times\mathbb{R}$

$$\frac{1}{2}\min_{\sigma\in\Sigma}\lambda_m(W(q,\sigma,t)+W^\top(q,\sigma,t))\geq\rho_W$$

with

$$W(q,\sigma,t)=\check{B}(q,\sigma,t)+\check{H}(q,\sigma,t)B(q,\sigma,t).$$

Remark 9. Note that W is synthesized by M and B. The inequality of W implies that the minimum eigenvalue of symmetric matrix $(W+W^\top)$ over the domain of uncertainty σ should not be smaller than a constant $\rho_W>-1$. For extreme cases, if M has no uncertainty, then the assumption is imposed to $W=\check{B}$; If furthermore, B has no uncertainty, then $W=0$, and the assumption can be removed. Therefore, this assumption simply specifies how many uncertainties in M and B can be tolerated in the control design, which is standard. ◀

Assumption 6. There exists a (possibly unknown) constant vector $\alpha\in(0,\infty)^k$ with $k\in\mathbb{N}_+$ and a known function $\Pi(\cdot):(0,\infty)^k\times\mathbb{R}^n\times\mathbb{R}^n\times\mathbb{R}\times\mathbb{R}\to\mathbb{R}_+$ such that for all $(q,\dot{q},t)\in$

$\mathbb{R}^n \times \mathbb{R}^n \times \mathbb{R}_+$,

$$(1+\rho_W)^{-1}\max_{\sigma\in\Sigma}\|\breve{H}(q,\sigma,t)(-C(q,\dot{q},\sigma,t)\dot{q} - g(q,\dot{q},\sigma,t) + B(q,\sigma,t)p_1(q,\dot{q},w,t)) + (\breve{B}(q,\sigma,t)p_1(q,\dot{q},w,t) - \breve{C}(q,\dot{q},\sigma,t)\dot{q} - \breve{g}(q,\dot{q},\sigma,t))\| \le \Pi(\alpha,q,\dot{q},w,t). \tag{20}$$

Furthermore, the function Π can be linearly factored with respect to α,

$$\Pi(\alpha,q,\dot{q},w,t) = \alpha^\top \breve{\Pi}(q,\dot{q},w,t),$$

where $\breve{\Pi}(\cdot) : \mathbb{R}^n \times \mathbb{R}^n \times \mathbb{R} \times \mathbb{R} \to \mathbb{R}^k_+$.

Remark 10. Since $\rho_W > -1$, we have $\rho_W + 1 > 0$. Note that the left-hand side of inequality (20) encompasses all system uncertainties, thus the function Π serves as a comprehensive bound for system uncertainties, capturing their collective effect. While the structure of Π is known, the constant vector α is possibly unknown since it is relevant to the unknown bounding set Σ. Therefore, Assumption 6 simply aims to provide a functional envelope by Π to characterize the worst-case effect of system uncertainties. ◀

The adaptive robust path following control is proposed as:

$$\tau(t) = p_1(q(t),\dot{q}(t),w(t),t) + p_2(q(t),\dot{q}(t),w(t),t) + p_3(\hat{\alpha}(t),q(t),\dot{q}(t),w(t),t). \tag{21}$$

Here, $p_{1,2}$ are given in (16), and p_3 is designed as

$$p_3(\hat{\alpha},q,\dot{q},w,t) = -\eta(\hat{\alpha},q,\dot{q},w,t)\upsilon(\hat{\alpha},q,\dot{q},w,t)\Pi(\hat{\alpha},q,\dot{q},w,t), \tag{22}$$

where

$$\upsilon = \bar{B}^\top \bar{M}^{-1} A^\top P\beta\Pi, \quad \eta = \begin{cases} \frac{1}{\|\upsilon\|}, & \text{if } \|\upsilon\| > \mu, \\ \frac{1}{\mu}, & \text{otherwise}, \end{cases} \tag{23}$$

and μ is a positive scalar constant. The parameter vector $\hat{\alpha} \in \mathbb{R}^k$ is governed by the following adaptive law:

$$\dot{\hat{\alpha}} = \begin{cases} \ell_1 \breve{\Pi}\|\breve{\beta}\| - \ell_2\hat{\alpha}, & \text{if } \|\breve{\Pi}\|\|\breve{\beta}\| > \varepsilon, \\ \ell_1 \breve{\Pi}\frac{\|\breve{\Pi}\|\|\breve{\beta}\|^2}{\varepsilon} - \ell_2\hat{\alpha}, & \text{otherwise}, \end{cases} \tag{24}$$

where ε, $\ell_{1,2}$ are positive scalar constants, $\hat{\alpha}_i(t_0) > 0$ and $\breve{\beta} = \bar{B}^\top D A^\top P\beta$. Hence $\upsilon = \breve{\beta}\Pi$.

Remark 11. The piecewise continuous adaptive law (24) is of leakage type, and the second term on the RHS is the leak. We can obtain $\hat{\alpha}_i(t) > 0$ for all $t \ge t_0$ with $\hat{\alpha}_i(t_0) > 0$. This is because the first term on the RHS is always non-negative, and by the property of differential inequality, the solution of (24) is always no less than that of $\dot{\hat{\alpha}} = -\ell_2\hat{\alpha}$ with $\hat{\alpha}_i(t_0) > 0$, which is always positive. The adaptive parameter $\hat{\alpha}$ tends to emulate the unknown α in the bound function Π, which will be proved in Theorem 2. As p_3 is designed based on $\hat{\alpha}$, it is called adaptive robust action. Consequently, the resulting control τ consisting of $p_{1,2,3}$ is called adaptive robust path-following control. This control design operates free from limitations on the system's number of degrees of freedom, making it suitable for a wide range of practical applications. ◀

Theorem 2 (Boundedness of uncertain system)**.** *Under Assumptions 3-6, the adaptive robust path-following control* (21) *ensures that, for the uncertain mechanical system* (1) *with the desired path* (10)*, both the path-following error* $\mathrm{dist}(\zeta(t),\mathcal{P})$ *and the adaptive error* $\|\hat{\alpha}(t) - \alpha\|$ *are uniformly ultimately bounded.*

Proof. See the Appendix. □

Remark 12. From the proof of Theorem 2, the boundedness region is primarily determined by the gain parameter κ, the matrix P, and the adaptive-law parameters $\ell_{1,2}$. These four factors collectively influence the extent of boundedness. Notably, for fixed P and $\ell_{1,2}$, the expression characterizing boundedness indicates that increasing κ tends to shrink—and never enlarges—the boundedness region. Hence, larger κ can enhance path-following accuracy. Moreover, while the main results are derived using the singularity-free GVF, they are also directly applicable to the general GVF presented in [4]. In fact, such application is even more straightforward, as it circumvents the need for the virtual state w. ◀

IV. Simulation Examples

This section presents simulations on an underactuated planar vertical take-off and landing (PVTOL) aircraft [19] for demonstrations. The corresponding dynamic model is [19]

$$\begin{aligned} m(t)\ddot{x}(t) &= -(\sin\theta(t))\tau_1(t) + (\cos\theta(t))\tau_2(t) + d_x(t), \\ m(t)\ddot{y}(t) &= (\cos\theta(t))\tau_1(t) + (\sin\theta(t))\tau_2(t) - m(t)g_0 + d_y(t), \\ J(t)\ddot{\theta}(t) &= \tau_2(t) + d_\theta(t), \end{aligned} \tag{25}$$

where states (x,y) and θ represent respectively the position and roll angle, control inputs τ_1 and τ_2 are respectively the thrust force and rolling torque, m and J are respectively the mass and the moment of inertia containing time-varying uncertainties, $d_{x,y,\theta}$ are unknown external disturbances, g_0 is the gravitational acceleration. The uncertain parameters m and J can be decomposed as $m(t) = \bar{m} + \Delta m(t)$, $J(t) = \bar{J} + \Delta J(t)$. The nominal PVTOL aircraft system can be obtained as

$$\begin{aligned} \bar{m}\ddot{x} &= -(\sin\theta)\tau_1 + (\cos\theta)\tau_2, \\ \bar{m}\ddot{y} &= (\cos\theta)\tau_1 + (\sin\theta)\tau_2 - \bar{m}g_0, \\ \bar{J}\ddot{\theta} &= \tau_2. \end{aligned} \tag{26}$$

Let $q := [x,y,\theta]^\top$. It is straightforward to cast (25) and (26) into the form of (1) and (15), respectively. The particular expressions of M, C, g, B and $\bar{M}$, $\bar{C}$, $\bar{g}$, $\bar{B}$ in this case are:

$$M = \begin{bmatrix} m & 0 & 0 \\ 0 & m & 0 \\ 0 & 0 & J \end{bmatrix}, \ \bar{M} = \begin{bmatrix} \bar{m} & 0 & 0 \\ 0 & \bar{m} & 0 \\ 0 & 0 & \bar{J} \end{bmatrix},$$

$$C = \bar{C} = \begin{bmatrix} 0 & 0 & 0 \\ 0 & 0 & 0 \\ 0 & 0 & 0 \end{bmatrix}, \ g = \begin{bmatrix} -d_x \\ mg_0 - d_y \\ -d_\theta \end{bmatrix},$$

$$\bar{g} = \begin{bmatrix} 0 \\ \bar{m}g_0 \\ 0 \end{bmatrix}, \ B = \bar{B} = \begin{bmatrix} -\sin\theta & \cos\theta \\ \cos\theta & \sin\theta \\ 0 & 1 \end{bmatrix}.$$

Three different desired paths are considered, i.e., the non-closed sinusoidal path $\mathcal{P}_1 = \{(x,y) \in \mathbb{R}^2 : y = \sin x\}$, the closed Cassini's oval $(x^2+y^2+r_a^2)^2 - 4r_a^2x^2 - r_b^4 = 0$ where $r_a = 3$, $r_b = 1.05r_a$, and the self-intersecting lemniscate of Bernoulli $\mathcal{P}_3 = \{(x,y) \in \mathbb{R}^2 : (x^2+y^2)^2 = x^2 - y^2\}$. To apply VFCFC, $\mathcal{P}_1$, $\mathcal{P}_2$, and $\mathcal{P}_3$ are respectively parameterized as: $\mathcal{P}_1^{hgh} = \{(x,y,w) \in \mathbb{R}^3 : x = w, y = \sin w\}$, $\mathcal{P}_2^{hgh} = \{(x,y,w) \in \mathbb{R}^3 : x = \cos(\omega)\sqrt{r_a^2\cos(2\omega) + \sqrt{r_b^4 - r_a^4\sin^2(2\omega)}}, y = \sin(\omega)\sqrt{r_a^2\cos(2\omega) + \sqrt{r_b^4 - r_a^4\sin^2(2\omega)}}\}$, $\mathcal{P}_3^{hgh} =$

$\{(x,y,w) \in \mathbb{R}^3 : x = \frac{\cos w}{1+\sin^2 w},\ y = \frac{\cos w \sin w}{1+\sin^2 w}\}$. As presented in (13), all three VFCs for $\mathcal{P}_{1,2,3}$ can be readily constructed with $A = \begin{bmatrix} 1 & 0 & 0 \\ 0 & 1 & 0 \end{bmatrix}$ that is of full row rank, and the particular expressions of $\tilde{\chi}$ are omitted here for simplicity. Therefore, we have

$$A\bar{M}^{-1}\bar{B} = \frac{1}{\bar{m}} \begin{bmatrix} -\sin\theta & \cos\theta \\ \cos\theta & \sin\theta \end{bmatrix}$$

for all three paths. Assumptions 1–4 can be verified for all three paths straightforwardly. Regarding Assumption 5, we have

$$\begin{aligned} W &= \check{H}B + \check{B} = (A\bar{M}^{-1}\bar{B})^{-1}A\bar{M}^{-1}(\bar{M}M^{-1} - I)B \\ &\quad + (A\bar{M}^{-1}\bar{B})^{-1}A\bar{M}^{-1}\Delta B = \left(\frac{\bar{m}}{m} - 1\right) I. \end{aligned}$$

Therefore, Assumption 5 can be verified, since

$$\frac{1}{2}\min_{\sigma\in\Sigma} \lambda_m(W + W^\top) = \min_{\sigma\in\Sigma}\left(\frac{\bar{m}}{m} - 1\right) > -1.$$

Regarding Assumption 6, the inequality (20) is deduced as follows:

$$\begin{aligned} &(1+\rho_W)^{-1}\max_{\sigma\in\Sigma}\|\check{H}(-C\dot{q} - g + Bp_1) + (\check{B}p_1 - \check{C}\dot{q} - \check{g})\| \\ &= (1+\rho_W)^{-1}\max_{\sigma\in\Sigma}\|-\check{H}(C\dot{q} + g) - (\check{C}\dot{q} - \check{g}) + (\check{H}B \\ &\quad + \check{B})p_1)\| \\ &= (1+\rho_W)^{-1}\max_{\sigma\in\Sigma}\|-(A\bar{M}^{-1}\bar{B})^{-1}A\bar{M}^{-1}H(C\dot{q} + g) \\ &\quad - (A\bar{M}^{-1}\bar{B})^{-1}A\bar{M}^{-1}(C\dot{q} + g) + Wp_1\| \\ &= (1+\rho_W)^{-1}\max_{\sigma\in\Sigma}\|-(A\bar{M}^{-1}\bar{B})^{-1}A\bar{M}^{-1}(H + I)(C\dot{q} \\ &\quad + g) + Wp_1\| \\ &\le (1+\rho_W)^{-1}\max_{\sigma\in\Sigma}\|(H+I)(C\dot{q} + g)\|\|(A\bar{M}^{-1}\bar{B})^{-1}A\bar{M}^{-1}\| \\ &\quad + (1+\rho_W)^{-1}\max_{\sigma\in\Sigma}\|W\|\|p_1\|. \end{aligned}$$

Therefore, we choose Π as

$$\Pi(\alpha, q, \dot{q}, \omega, t) = \alpha^\top \breve{\Pi}(q, \dot{q}, \omega, t) := [\alpha_1\ \alpha_2] \begin{bmatrix} \breve{\Pi}_1(q, \dot{q}, t) \\ \breve{\Pi}_2(q, \dot{q}, \omega, t) \end{bmatrix},$$

where $\alpha_1 = (1+\rho_W)^{-1}\max_{\sigma\in\Sigma}\|(H+I)(C\dot{q}+g)\|$, $\alpha_2 = (1+\rho_W)^{-1}\max_{\sigma\in\Sigma}\|W\|$, $\breve{\Pi}_1 = \|(A\bar{M}^{-1}\bar{B})^{-1}A\bar{M}^{-1}\|$, $\breve{\Pi}_2 = \|p_1\|$. Both α_1 and α_2 are unknown as the uncertainty bound is unknown.

For simulations, system parameters and uncertainties are chosen as $\bar{m} = 1\text{kg}$, $\bar{J} = 0.5\text{kg}\cdot\text{m}^2$, $\Delta m(t) = 0.3\bar{m}\sin(5t)$, $\Delta J(t) = 0.3\bar{J}\sin(7.5t)$, $d_x(t) = 4\sin(2t)$, $d_y(t) = 4\cos(4t)$, $d_\theta(t) = 4\sin(6t)$, $x(0) = 2.2$ m, $y(0) = 0.2$ m, $\theta(0) = 1.5$ rad, $\dot{x}(0) = 1$ m/s, $\dot{y}(0) = 0$, $\dot{\theta}(0) = 0$. The simulations are implemented in two steps, with the first step testing the nominal VFCFC (NVFCFC) (16) for nominal system (26), and the second step testing the adaptive robust VFCFC (ARVFCFC) (21) for uncertain system (25).

In the first step, the control parameters of NVFCFC are chosen as $k_1 = k_2 = 1$, P the identity matrix, $\kappa = 5$, $\omega(0) = 0.1$. The conventional CFC (CCFC), and the immersion and invariance-based orbital stabilization (IIOS) in [20] are also tested for comparisons. When applying the CCFC design, the indispensable Assumption 1 can be satisfied by the resulting constraint to encode $\mathcal{P}_1$, but cannot be satisfied by the resulting constraint to encode $\mathcal{P}_2$ and $\mathcal{P}_3$. Specifically, by invoking the constraint design method of CCFC presented in "Motivated solution strategy" of Section II-D, one obtains constraints to encode $\mathcal{P}_2$ and $\mathcal{P}_3$ whose second-order forms as (4) have no solution for $(\ddot{x}, \ddot{y})$ at $(x, y, \dot{x}, \dot{y}) = (0, 0, 0, 0)$, violating Assumption 1. On the other hand, IIOS in [20] is only applicable to non-intersecting closed paths, therefore it is only tested on $\mathcal{P}_2$.

Figs.1–IV show the simulation results of the first step. It shows that NVFCFC completes all three path-following tasks with vanishing path-following errors. Furthermore, NVFCFC exhibits a certain degree of robustness to system parameter variations (Fig. IV). Despite showing faster error convergence compared with NVFCFC, CCFC fails the path-following task of $\mathcal{P}_1$ since the system trajectory moves back and forth in the neighborhood of some point on the desired path after convergence (Fig.1), thereby it fails any of the three path-following tasks. IIOS only completes the path-following task of $\mathcal{P}_2$, but produces a larger path-following error after convergence compared with NVFCFC, despite consuming significantly higher control effort (Fig. 3).

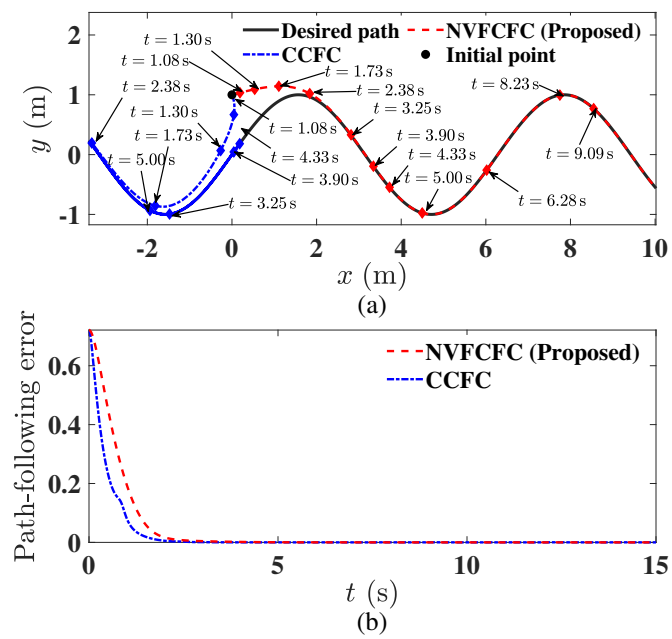

Fig. 1. These are three τ

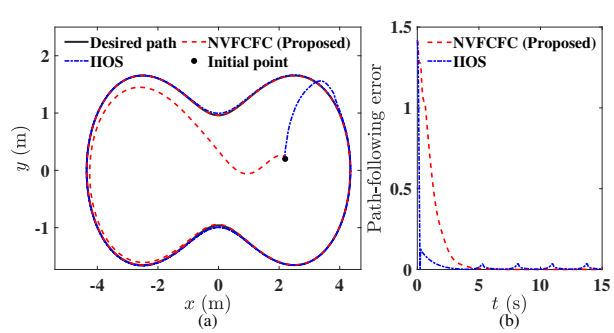

Fig. 2. These are three τ

In the second step, the control parameters of p_3 in ARVFCFC are chosen as $\ell_1 = 0.5$, $\ell_2 = 0.1$, $\varepsilon = 1$. Other parameters are chosen to be the same as those in NVFCFC. NVFCFC and IIOS are also tested for comparisons. Figs. 5–8 show the corresponding simulation results. It shows

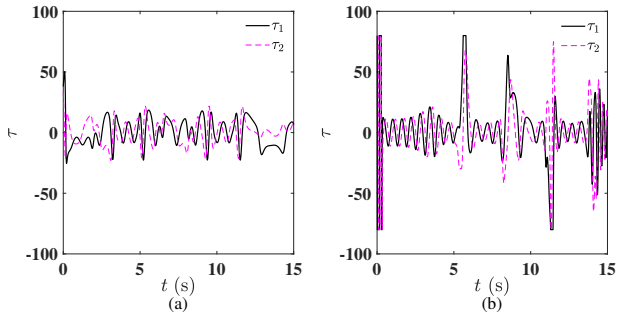

Fig. 3. NVFCFC and IIOS of the nominal PVTOL aircraft system.

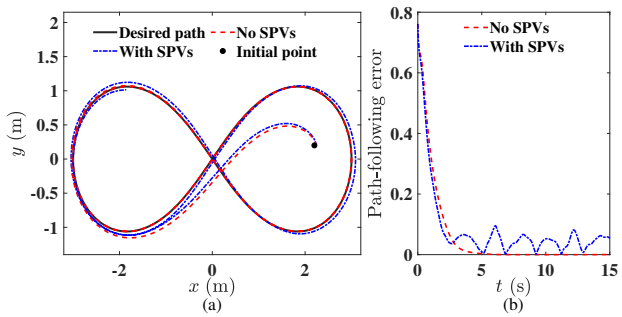

Fig. 4. These are three $\boldsymbol{\tau}$

that ARVFCFC completes all three path-following tasks with ultimately bounded path-following errors. After some time adaptive parameters $\hat{\alpha}_{1,2}$ enter some positive region, consistent with Theorem 2 (Figs. 5(b), 6(b), 7(b)). NVFCFC fails the path-following task of $\mathcal{P}_3$ since the system trajectory significantly deviates from $\mathcal{P}_3$ (Fig. 6). This reflects the effectiveness of incorporating p_3 to address uncertainties. IIOS completes the path-following task of $\mathcal{P}_2$, but produces a significantly larger path-following error after convergence compared with ARVFCFC, despite consuming significantly higher control effort (Figs.8).

A. A fully-actuated 3-link space manipulator system

The dynamic model of a fully-actuated 3-link space manipulator [21] can be put in the form of (1) with

$$M = \begin{bmatrix} m_{12} & 0 & 0 \\ 0 & m_{22} & m_{23} \\ 0 & m_{32} & m_{33} \end{bmatrix}, C\dot{q} = \begin{bmatrix} C_1 \\ C_2 \\ C_3 \end{bmatrix}, g = \begin{bmatrix} d_{\theta_1} \\ g_2 + d_{\theta_2} \\ g_3 + d_{\theta_3} \end{bmatrix},$$
$$B = \begin{bmatrix} 1 & 0 & 0 \\ 0 & 1 & 0 \\ 0 & 0 & 1 \end{bmatrix}, \tau = \begin{bmatrix} \tau_1 \\ \tau_2 \\ \tau_3 \end{bmatrix}.$$

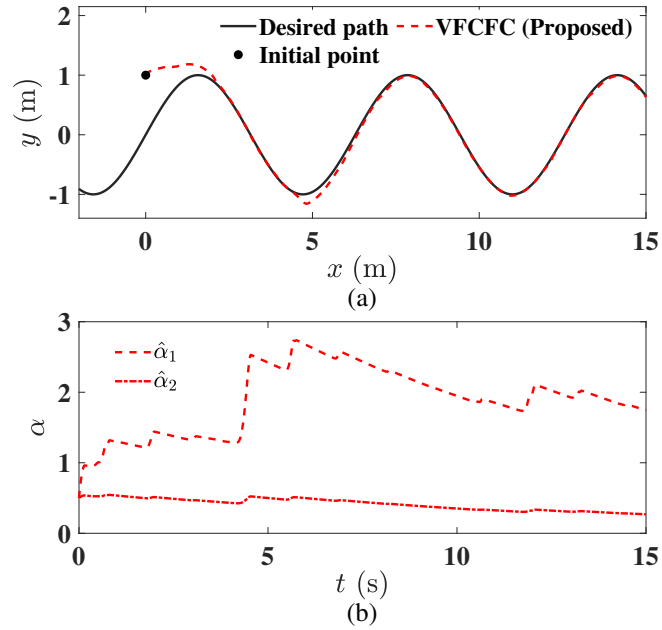

Fig. 5. x.

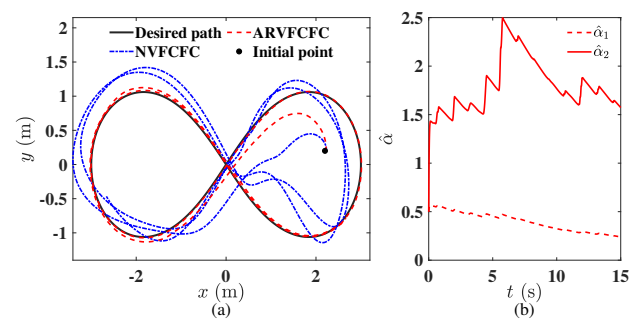

Fig. 6. x.

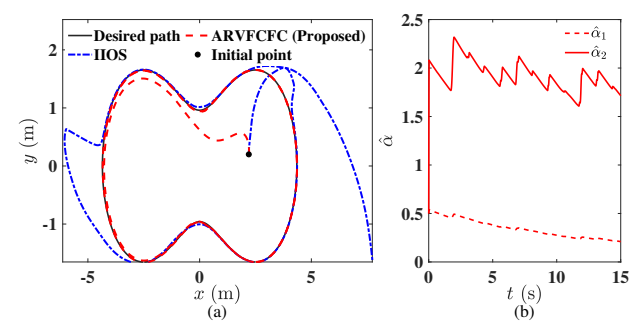

Fig. 7. x.

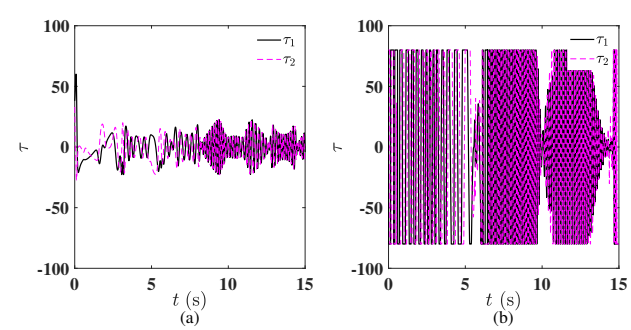

Fig. 8. ARVFCFC and IIOS of the uncertain PVTOL aircraft system.

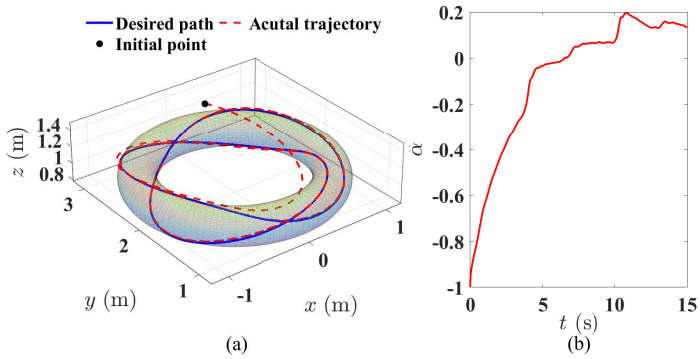

Fig. 9. ARVFCFC of the uncertain LRA.

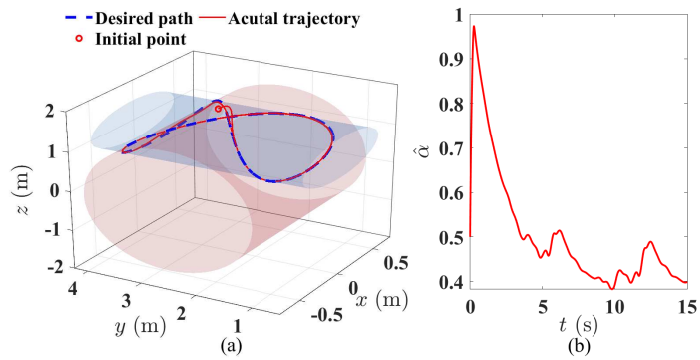

Fig. 10. ARVFCFC of the uncertain LRA.

Here,

$$
\begin{aligned}
&m_{12} = m_3 l_2^2 c_{23}^2 + 2m_3 l_1 l_2 c_2 c_{23} + m_2 m_3 l_1^2 c_2^2 + J,\\
&m_{22} = m_3 l_2^2 + 2m_3 l_1 l_2 c_3 + (m_2+m_3) l_1^2,\\
&m_{23} = m_{32} = m_3 l_2 (l_1 + l_2 c_3), m_{33} = m_3 l_2^2,\\
&C_1 = -2m_3 l_2^2 \dot\theta_1 \dot\theta_2 s_{23} c_{23} - 2m_3 l_2^2 \dot\theta_1 \dot\theta_3 s_{23} c_{23}\\
&\quad - 2m_3 l_1 l_2 \dot\theta_1 \dot\theta_2 s_2 c_{23} - 2m_3 l_1 l_2 \dot\theta_1 \dot\theta_2 c_2 s_{23}\\
&\quad - 2m_3 l_1 l_2 \dot\theta_1 \dot\theta_3 c_2 s_{23} - 2(m_2+m_3) l_1^2 \dot\theta_1 \dot\theta_2 s_2 c_2,\\
&C_2 = m_3 l_2^2 \dot\theta_1^2 s_{23} c_{23} + m_3 l_1 l_2 \dot\theta_2^2 s_3 + m_3 l_1 l_2 \dot\theta_2^2 c_2 s_{23}\\
&\quad - m_3 l_1 l_2 \dot\theta_1^2 c_{23}^2 s_3 - m_3 l_1 l_2 (\dot\theta_2 + \dot\theta_3)^2 s_3\\
&\quad + m_3 l_1 l_2 \dot\theta_1^2 s_{23} c_{23} c_3 + (m_2+m_3) l_1^2 \dot\theta_1^2 s_2 c_2,\\
&C_3 = m_3 l_2^2 \dot\theta_1^2 s_{23} c_{23} + m_3 l_1 l_2 \dot\theta_2^2 s_3 + m_3 l_1 l_2 \dot\theta_1^2 c_2 s_{23},\\
&g_2 = m_3 g_0 l_2 c_{23} + (m_2+m_3) g l_1 c_2, g_3 = m_3 g_0 l_2 c_{23},
\end{aligned}
$$

and $q = [\theta_1, \theta_2, \theta_3]^\top$ are the angles of links of the manipulator, $\tau = [\tau_1, \tau_2, \tau_3]^\top$ respectively represent the control torture imposed on the links, l_1 is the length of link 2, l_2 is the length of link 3, J is the the rotary inertia of link 1, m_2, m_3 are the masses of link 2 and 3, respectively, $s_i = \sin\theta_i$, $c_i = \cos\theta_i$, $i = 2, 3$, $s_{23} = \sin(\theta_2 + \theta_3)$, $c_{23} = \cos(\theta_2 + \theta_3)$, g_0 is the gravitational acceleration. Furthermore, d_{θ_1}, d_{θ_2}, and d_{θ_3} are unknown external disturbances, and $m_i (i = 2, 3)$ and J are considered to contain uncertainties, which can be decomposed as $m_i = \bar m_i + \Delta m_i$, $J = \bar J + \Delta J$. These uncertainties are all bounded with unknown bounds.

Denote the coordinates of the end effector of the manipulator as $[x, y, z]$, for which we choose a self-intersecting desired path $\mathcal{P}$ in 3-D that is the intersection of two cylinders described by $(x - x^c)^2 + (z - z^c)^2 = R_1^2$ and $(y - y^c)^2 + z^2 = R_2^2$. We can find a parametrization for the desired path as follows:

$$
\begin{aligned}
x &= f_1(w) = x^c + R_1 \sin(2w),\\
y &= f_2(w) = y^c + 2\sin w \sqrt{R_1(R_2 - R_1 \sin^2 w)},\\
z &= f_3(w) = z^c + R_1 \cos(2w).
\end{aligned} \tag{27}
$$

We choose $R_2 = 1.5, R_1 = 0.5, x^c = 0, y^c = 2.5, z^c = R_2 - R_1 = 1$. To further evaluate the proposed method, we consider another desired path given by a non-self-intersecting torus knot, described by

$$
\begin{aligned}
x &= f_1(w) = a + (R_0 + r_0 \cos(q1 * th)) \cos(q_2 \omega),\\
y &= f_2(w) = b + (R_0 + r_0 \cos(q1 * th)) \sin(q_2 \omega),\\
z &= f_3(w) = c + r_0 \sin(q_1 \omega);
\end{aligned}
$$

where $R_0 = 1$, $r_0 = 0.2$, $q_1 = 3$, $q_2 = 2$, $a = 0$, $b = 2$, and $c = 1$. In particular, this path corresponds to a $(3, 2)$-torus knot. Since the path-following task is directly assigned to the end effector of the manipulator, while the system model is established by the link angles θ_1, θ_2 and θ_3, we need to invoke the analytical expressions that relate the angles $[\theta_1, \theta_2, \theta_3]$ to the end effector coordinates $[x, y, z]$, which are:

$$
\begin{aligned}
&\theta_1 = \arctan \frac{x}{y},\\
&\theta_2 = \arccos \frac{x^2 + y^2 + z^2 - l_1^2 - l_2^2}{2 l_1 \sqrt{x^2 + y^2 + z^2}} + \arccos \sqrt{\frac{x^2 + y^2}{x^2 + y^2 + z^2}},\\
&\theta_3 = \arccos \frac{x^2 + y^2 + z^2 - l_1^2 - l_2^2}{2 l_1 l_2}.
\end{aligned} \tag{28}
$$

Combining (27) and (28), the corresponding VFC encoding the desired path for $[x, y, z]$, can be obtained by (13) with $A = I_{3\times 3}$, and the particular expression of $\tilde\chi$ is omitted here.

Similar to assumptions verification for PVTOL, Assumptions 1–4 can be verified straightforwardly. Assumption 5 can be verified by $W = \bar M M^{-1}$ indicating $\frac{1}{2}\min_{\sigma\in\Sigma} \lambda_m(W + W^\top) > 0$. Regarding the inequality (20) in Assumption 6, note that the terms in M, $C\dot q$, and g are either constant, bounded by a constant, trigonometric in positions, or quadratic in velocities; besides, there are additional terms corresponding to the VFC that are constant, or trigonometric in ω. Therefore, to meet Assumption 6, we choose

$$
\Pi(\alpha, q, \dot q, t) = \alpha(\|\dot q\|^2 + \|\dot q\| + 1) =: \alpha \breve\Pi(q, \dot q, t), \tag{29}
$$

where $\alpha \in \mathbb{R}_+$. For simulations, we choose $\bar J = 0.5\,\mathrm{kg}\cdot\mathrm{m}^2$, $\bar m_2 = 1\,\mathrm{kg}$, $\bar m_3 = 2\,\mathrm{kg}$ and the initial conditions are $\theta_1(0) = -0.1\,\mathrm{rad}$, $\theta_2(0) = 1.5\,\mathrm{rad}$, $\theta_3(0) = 1.5\,\mathrm{rad}$, $\dot\theta_1(0) = 1\,\mathrm{rad/s}$, $\dot\theta_2(0) = 0$, $\dot\theta_3(0) = 0$, $\alpha(0) = 0.5$, $\omega(0) = 0$. The uncertainties are simulated by $\Delta J = 0.1\bar J \sin(7.5t)$, $\Delta m_2 = 0.1\bar m_2 \sin(5t)$, $\Delta m_3 = 0.1\bar m_3 \cos(5t)$, $d_{\theta_1} = 3\sin 2t$, $d_{\theta_2} = 3\cos 4t$, $d_{\theta_3} = 3\sin 6t$. The VFC and control parameters are chosen as $k_1 = k_2 = k_3 = 1$, $P = I$, $\kappa = 5$, $\ell_1 = 0.5$, $\ell_2 = 0.3$, $\varepsilon = 1$.

The simulation results are presented in Figs. 9–10. The trajectory of the manipulator system presented in Figs. 9(a) and 10(a) finally (approximately) follows the desired path. Fig. 9(b) and 10(b) shows the evolution of the adaptive parameter $\hat\alpha$.

V. Conclusion

This note integrates GVF and CFC to solve the dynamics control problem of geometric path-following for mechanical systems under heterogeneous time-varying uncertainties–a task impossible with either approach alone. The VFC is meticulously constructed to encode the desired path, bridging GVF and CFC. Under mild assumptions, the main results include: i) path-following error convergence matches that of the VFC-following error; ii) nominal VFCFC ensures vanishing errors without uncertainties; iii) adaptive robust VFCFC ensures ultimately bounded errors with uncertainties. Simulations on a PVTOL aircraft validate the approach.

This work opens a new avenue for path-following control that considers the internal dynamics of uncertain systems. Future research may explore extensions such as collision avoidance, input saturation, and time-varying desired paths in swarm mechanical systems, for enhanced robotic deployment.

References

[1] A. P. Aguiar, J. P. Hespanha, and P. V. Kokotović, "Performance limitations in reference tracking and path following for nonlinear systems," *Automatica*, vol. 44, no. 3, pp. 598–610, 2008.

[2] P. Sujit, S. Saripalli, and J. B. Sousa, "Unmanned aerial vehicle path following: A survey and analysis of algorithms for fixed-wing unmanned aerial vehicless," *IEEE Control Systems Magazine*, vol. 34, no. 1, pp. 42–59, 2014.

[3] V. M. Goncalves, L. C. Pimenta, C. A. Maia, B. C. Dutra, and G. A. Pereira, "Vector fields for robot navigation along time-varying curves in n-dimensions," *IEEE Transactions on Robotics*, vol. 26, no. 4, pp. 647–659, 2010.

[4] W. Yao and M. Cao, "Path following control in 3d using a vector field," *Automatica*, vol. 117, no. 108957, pp. 1–9, 2020.

[5] B.-B. Hu, H.-T. Zhang, W. Yao, Z. Sun, and M. Cao, "Coordinated guiding vector field design for ordering-flexible multi-robot surface navigation," *IEEE Transactions on Automatic Control*, vol. 69, no. 7, pp. 4805–4812, 2024.

[6] Y. A. Kapitanyuk, A. V. Proskurnikov, and M. Cao, "A guiding vector-field algorithm for path-following control of nonholonomic mobile robots," *IEEE Transactions on Control Systems Technology*, vol. 26, no. 4, pp. 1372–1385, July 2018.

[7] W. F. Phillips, *Mechanics of flight*. John Wiley & Sons, 2004.

[8] Y.-H. Chen, "Constraint-following servo control design for mechanical systems," *Journal of Vibration and Control*, vol. 15, no. 3, pp. 369–389, 2009.

[9] Y.-H. Chen and X. Zhang, "Adaptive robust approximate constraint-following control for mechanical systems," *Journal of the Franklin Institute*, vol. 347, no. 1, pp. 69–86, Feb. 2010.

[10] A. H. Bajodah, D. H. Hodges, and Y.-H. Chen, "Inverse dynamics of servo-constraints based on the generalized inverse," *Nonlinear Dynamics*, vol. 39, p. 179–196, 2005.

[11] F. E. Udwadia and R. E. Firdaus, "Optimal tracking control of nonlinear dynamical systems," *Proceedings of the Royal Society A: Mathematical, Physical and Engineering Sciences*, vol. 464, no. 2097, pp. 2341–2363, 2008.

[12] F. E. Udwadia and H. Mylapilli, "Constrained motion of mechanical systems and tracking control of nonlinear systems: Connections and closed-form results," *Nonlinear Dynamics and Systems Theory*, vol. 15, no. 1, pp. 73–89, 2015.

[13] H. Khalil, *Nonlinear Systems*, 3rd ed. Prentice Hall, 2002.

[14] Z. Zhang, C. Wen, L. Xing, and Y. Song, "Adaptive output feedback control of nonlinear systems with mismatched uncertainties under input/output quantization," *IEEE Transactions on Automatic Control*, vol. 67, no. 9, pp. 4801–4808, 2022.

[15] W. Yao, H. G. de Marina, B. Lin, and M. Cao, "Singularity-free guiding vector field for robot navigation," *IEEE Transactions on Robotics*, vol. 37, no. 4, pp. 1206–1221, 2021.

[16] P. Ioannou and B. Fidan, *Adaptive control tutorial*. Society for Industrial and Applied Mathematics, 2006.

[17] H. Yin, Y.-H. Chen, and D. Yu, "Controlling an Underactuated Two-Wheeled Mobile Robot: A Constraint-Following Approach," *Journal of Dynamic Systems, Measurement, and Control-Transactions of the ASME*, vol. 141, no. 7, p. 071002, Jul. 2019.

[18] H. Yin, Y.-H. Chen, J. Huang, and H. Lü, "Tackling mismatched uncertainty in robust constraint-following control of underactuated systems," *Information Sciences*, vol. 520, pp. 337–352, 2020.

[19] C. Aguilar-Ibáñez, J. H. Sossa-Azuela, and M. S. Suarez-Castanon, "A backstepping-based procedure with saturation functions to control the pvtol system," *Nonlinear Dynamics*, vol. 83, no. 3, pp. 1247–1257, 2016.

[20] B. Yi, R. Ortega, I. R. Manchester, and H. Siguerdidjane, "Path following of a class of underactuated mechanical systems via immersion and invariance-based orbital stabilization," *International Journal of Robust and Nonlinear Control*, vol. 30, p. 8521–8544, 2020.

[21] L. Shi, J. Katupitiya, and N. Kinkaid, "A robust attitude controller for a spacecraft equipped with a robotic manipulator," in *2016 American Control Conference (ACC)*. IEEE, 2016, pp. 4966–4971.

[22] M. Corless and G. Leitmann, "Continuous state feedback guaranteeing uniform ultimate boundedness for uncertain dynamic systems," *IEEE Transactions on Automatic Control*, vol. 26, no. 5, pp. 1139–1144, 1981.

Appendix

Proof of Theorem 2

Let

$$V(\beta, \hat{\alpha}-\alpha) = \beta^\top P\beta + \ell_1^{-1}(1+\rho_W)(\hat{\alpha}-\alpha)^\top(\hat{\alpha}-\alpha)$$

be the Lyapunov function candidate. The time derivative of V is given by

$$\dot{V} = 2\beta^\top P\dot{\beta} + 2\ell_1^{-1}(1+\rho_W)(\hat{\alpha}-\alpha)^\top\dot{\hat{\alpha}}. \tag{30}$$

In the proof, the arguments of functions are mostly omitted when no confusion is likely to arise, except for a few critical cases. Now we deal with (30) by analyzing each term separately. First,

$$\begin{aligned} 2\beta^\top P\dot{\beta} &= 2\beta^\top P(A\ddot{q}-b) \\ &= 2\beta^\top P\{A[M^{-1}(B\tau - C\dot{q} - g)] - b\}. \end{aligned} \tag{31}$$

By the decomposition for nominal and uncertain portions of system matrices and $M^{-1} = \bar{M}^{-1} + (M^{-1} - \bar{M}^{-1})$, we can obtain

$$\begin{aligned} &\beta^\top P\{A[M^{-1}(B\tau - C\dot{q} - g)] - b\} \\ =&\beta^\top P\{A[\bar{M}^{-1}(-\bar{C}\dot{q} - \bar{g}) + \bar{M}^{-1}B(p_1+p_2) + \bar{M}^{-1}(-\Delta C\dot{q} \\ &- \Delta g) + (M^{-1} - \bar{M}^{-1})(-C\dot{q} - g + Bp_1 + Bp_2) \\ &+ M^{-1}Bp_3] - b\}. \end{aligned} \tag{32}$$

By $B = \bar{B} + \Delta B$, $\Delta B = \bar{B}\check{B} + \tilde{B}$ and p_1 in (17) we have

$$\begin{aligned} &A[\bar{M}^{-1}(-\bar{C}\dot{q} - \bar{g}) + \bar{M}^{-1}Bp_1] - b \\ =&A[\bar{M}^{-1}(-\bar{C}\dot{q} - \bar{g}) + \bar{M}^{-1}(\bar{B} + \bar{B}\check{B} + \tilde{B})p_1] - b \\ =&A[\bar{M}^{-1}(-\bar{C}\dot{q} - \bar{g}) + \bar{M}^{-1}\bar{B}p_1] - b + A\bar{M}^{-1}\bar{B}\check{B}p_1 \\ &+ A\bar{M}^{-1}\tilde{B}p_1 \\ =&A\bar{M}^{-1}\bar{B}\check{B}p_1. \end{aligned} \tag{33}$$

Then we look at the terms on the RHS of (32)

$$\begin{aligned}
&A[\bar{M}^{-1}(-\bar{C}\dot{q}-\bar{g})+\bar{M}^{-1}B(p_1+p_2)+\bar{M}^{-1}(-\Delta C\dot{q}-\Delta g)\\
&\quad+(M^{-1}-\bar{M}^{-1})(-C\dot{q}-g+Bp_1+Bp_2)]-b\\
=&A\bar{M}^{-1}\bar{B}\check{B}p_1+A[\bar{M}^{-1}Bp_2+\bar{M}^{-1}(-\Delta C\dot{q}-\Delta g)\\
&\quad+(M^{-1}-\bar{M}^{-1})(-C\dot{q}-g+Bp_1+Bp_2)]\\
=&A\{\bar{M}^{-1}[\bar{B}\check{B}p_1-(\bar{B}\check{C}+\tilde{C})\dot{q}-(\bar{B}\check{g}+\tilde{g})]\\
&\quad+\bar{M}^{-1}(\bar{B}\tilde{H}+\tilde{H})(-C\dot{q}-g+Bp_1+Bp_2)+\bar{M}^{-1}Bp_2\}\\
=&A\bar{M}^{-1}(\bar{B}\check{B}p_1-\bar{B}\check{C}\dot{q}-\bar{B}\check{g}+Bp_2)-A\bar{M}^{-1}(\tilde{C}\dot{q}\\
&\quad+\tilde{g})+A\bar{M}^{-1}\bar{B}\tilde{H}(-C\dot{q}-G+Bp_1+Bp_2)\\
&\quad+A\bar{M}^{-1}\tilde{H}(-C\dot{q}-g+Bp_1+Bp_2)\\
=&A\bar{M}^{-1}\bar{B}[\check{H}(-C\dot{q}-g+Bp_1)+(\check{B}p_1+-\check{C}\dot{q}\\
&\quad-\check{g})]+A\bar{M}^{-1}\bar{B}\check{H}Bp_2+A\bar{M}^{-1}Bp_2.
\end{aligned}\tag{34}$$

The last two terms on the RHS of (34) can be rewritten as:

$$\begin{aligned}
&A\bar{M}^{-1}\bar{B}\check{H}Bp_2+A\bar{M}^{-1}Bp_2\\
=&A\bar{M}^{-1}(H-\tilde{H})(\bar{B}+\Delta B)p_2+A\bar{M}^{-1}(\bar{B}+\Delta B)p_2\\
=&A\{M^{-1}+\bar{M}^{-1}[H-\bar{B}(A\bar{M}^{-1}\bar{B})^{-1}A\bar{M}^{-1}H]\}(\bar{B}\\
&\quad+\Delta B)p_2\\
=&AM^{-1}(\bar{B}+\Delta B)p_2.
\end{aligned}\tag{35}$$

By (31)-(35), we can obtain

$$\begin{aligned}
&2\beta^\top P\dot{\beta}=2\beta^\top PA\bar{M}^{-1}\bar{B}[\check{H}(-C\dot{q}-g+Bp_1)+(\check{B}p_1\\
&\quad-\check{C}\dot{q}-\check{g})]+2\beta^\top PAM^{-1}(\bar{B}+\Delta B)p_2\\
&\quad+2\beta^\top PAM^{-1}(\bar{B}+\Delta B)p_3.
\end{aligned}\tag{36}$$

Considering the first two terms on the RHS of (36), by Assumption 6, we have

$$\begin{aligned}
&2\beta^\top PA\bar{M}^{-1}\bar{B}[\check{H}(-C\dot{q}-g+Bp_1)+(\check{B}p_1\\
&\quad-\check{C}\dot{q}-\check{g})]\le 2\|\check{\beta}\|(1+\rho_W)\Pi(\alpha,q,\dot{q},w,t).
\end{aligned}$$

Considering the last two terms on the RHS of (36), we have

$$\begin{aligned}
&2\beta^\top PAM^{-1}(\bar{B}+\Delta B)p_2+2\beta^\top PAM^{-1}(\bar{B}+\Delta B)p_3\\
=&2\beta^\top PAM^{-1}(\bar{B}+\Delta B)(p_2+p_3),
\end{aligned}$$

where

$$\begin{aligned}
&2\beta^\top PAM^{-1}(\bar{B}+\Delta B)\\
=&2\beta^\top PA\bar{M}^{-1}[I+(\bar{B}\check{H}+\tilde{H})](\bar{B}+\bar{B}\check{B}+\tilde{B})\\
=&2\beta^\top P(A\bar{M}^{-1}\bar{B}+A\bar{M}^{-1}\bar{B}\check{B})+2\beta^\top PA\bar{M}^{-1}\bar{B}\check{H}(\bar{B}\\
&\quad+\bar{B}\check{B}+\tilde{B})\\
=&2\beta^\top PA\bar{M}^{-1}\bar{B}[I+\check{B}+\check{H}(\bar{B}+\bar{B}\check{B}+\tilde{B})]\\
=&2\beta^\top PA\bar{M}^{-1}\bar{B}(I+\check{B}+\check{H}B).
\end{aligned}$$

By p_2 in (16), we have

$$\begin{aligned}
&2\beta^\top PAM^{-1}(\bar{B}+\Delta B)p_2\\
=&2\beta^\top PA\bar{M}^{-1}\bar{B}(I+\check{B}+\check{H}B)(-\kappa(A\bar{M}^{-1}\bar{B})^\top P\beta)\\
=&2\beta^\top PA\bar{M}^{-1}\bar{B}(-\kappa\bar{B}^\top\bar{M}^{-1}A^\top P\beta)+2\beta^\top PA\bar{M}^{-1}\bar{B}\\
&\quad\times(\check{B}+\check{H}B)(-\kappa\bar{B}^\top\bar{M}^{-1}A^\top P\beta).
\end{aligned}$$

Applying Assumptions 4 and 5 yields

$$\begin{aligned}
&2\beta^\top PAM^{-1}(\bar{B}+\Delta B)p_2=-2\kappa\beta^\top(PA\bar{M}^{-1}\bar{B}\bar{B}^\top\\
&\quad\times\bar{M}^{-1}A^\top P)\beta-2\beta^\top PA\bar{M}^{-1}\bar{B}\frac{1}{2}(W+W^\top)\\
&\quad\times(\kappa B^\top\bar{M}^{-1}A^\top P\beta)\\
&\quad\le-2\kappa(1+\rho_W)\underline{\lambda}\|\beta\|^2.
\end{aligned}$$

Similarly, by p_3 in (22) we have

$$\begin{aligned}
&2\beta^\top PAM^{-1}(\bar{B}+\Delta B)p_3\\
=&2\beta^\top PA\bar{M}^{-1}\bar{B}(-\eta\upsilon\Pi(\alpha,q,\dot{q},w,t))+2\beta^\top PA\bar{M}^{-1}\\
&\quad\times\bar{B}(\check{B}+\check{H}B)(-\eta\upsilon\Pi(\hat{\alpha},q,\dot{q},w,t))\\
=&2\beta^\top PA\bar{M}^{-1}\bar{B}(-\eta\bar{B}^\top\bar{M}^{-1}A^\top P\beta\Pi^2(\hat{\alpha},q,\dot{q},w,))\\
&\quad+2\beta^\top PA\bar{M}^{-1}\bar{B}(\check{B}+\check{H}B)(-\eta\bar{B}^\top\bar{M}^{-1}A^\top P\beta\\
&\quad\times\Pi^2(\hat{\alpha},q,\dot{q},w,t)).
\end{aligned}\tag{37}$$

By (23), the first term on the RHS of (37) is

$$\begin{aligned}
&2\beta^\top PA\bar{M}^{-1}\bar{B}(-\eta\bar{B}^\top\bar{M}^{-1}A^\top P\beta\Pi^2(\hat{\alpha},q,\dot{q},w,t))\\
&=-2\eta\Pi(\hat{\alpha},q,\dot{q},w,t)\beta^\top PA\bar{M}^{-1}\bar{B}\bar{B}^\top\bar{M}^{-1}A^\top P\beta\\
&\quad\times\Pi(\hat{\alpha},q,\dot{q},w,t)\\
&=-2\eta\|\upsilon(\hat{\alpha},q,\dot{q},w,t)\|^2.
\end{aligned}\tag{38}$$

Based on Assumption 5, the second term on the RHS of (37) is

$$\begin{aligned}
&2\beta^\top PA\bar{M}^{-1}\bar{B}(\check{B}+\check{H}B)(-\eta\bar{B}^\top\bar{M}^{-1}A^\top P\beta\\
&\quad\times\Pi^2(\hat{\alpha},q,\dot{q},w,t))\\
&=-2\eta(\Pi(\hat{\alpha},q,\dot{q},w,t)\beta^\top PA\bar{M}^{-1}\bar{B}\frac{1}{2}(W+W^\top)(\bar{B}^\top\\
&\quad\times\bar{M}^{-1}A^\top P\beta\Pi(\hat{\alpha},q,\dot{q},w,t))\\
&\quad\le-2\eta\rho_W\|\upsilon(\hat{\alpha},q,\dot{q},w,t)\|^2.
\end{aligned}\tag{39}$$

Combining (37)-(39) we can obtain

$$2\beta^\top PAM^{-1}(\bar{B}+\Delta B)p_3\le-2\eta(1+\rho_W)\|\upsilon(\hat{\alpha},q,\dot{q},w,t)\|^2.$$

Based on (24), if $\|\upsilon\|>\mu$, $-2\eta(1+\rho_W)\|\upsilon\|^2=-2(1+\rho_W)\|\upsilon\|$ and

$$\begin{aligned}
&2\beta^\top P\dot{\beta}\le 2\|\check{\beta}\|(1+\rho_W)\Pi(\alpha,q,\dot{q},w,t)\\
&\quad-2\kappa(1+\rho_W)\underline{\lambda}\|\beta\|^2-2(1+\rho_W)\|\upsilon(\hat{\alpha},q,\dot{q},w,t)\|\\
=&2\|\check{\beta}\|(1+\rho_W)\Pi(\alpha,q,\dot{q},w,t)-2\kappa(1+\rho_W)\underline{\lambda}\|\beta\|^2\\
&\quad-2\|\check{\beta}\|(1+\rho_W)\Pi(\hat{\alpha},q,\dot{q},w,t)\\
=&-2\kappa(1+\rho_W)\underline{\lambda}\|\beta\|^2-2\|\check{\beta}\|(1+\rho_W)(\hat{\alpha}-\alpha)^\top\check{\Pi}(q,\dot{q},w,t).
\end{aligned}\tag{40}$$

And if $\|\upsilon\|\le\mu$, $-2\eta(1+\rho_W)\|\upsilon\|^2=-2(1+\rho_W)\|\upsilon\|^2/\mu$ and

$$\begin{aligned}
&2\beta^\top P\dot{\beta}\\
&\le 2\|\check{\beta}\|(1+\rho_W)\Pi(\alpha,q,\dot{q},w,t)-2\kappa(1+\rho_W)\underline{\lambda}\|\beta\|^2\\
&-2(1+\rho_W)\frac{\|\upsilon(\hat{\alpha},q,\dot{q},w,t)\|^2}{\mu}\\
&=2\|\check{\beta}\|(1+\rho_W)\Pi(\alpha,q,\dot{q},w,t)\\
&-2\kappa(1+\rho_W)\underline{\lambda}\|\beta\|^2-2(1+\rho_W)\frac{\|\upsilon(\hat{\alpha},q,\dot{q},w,t)\|^2}{\mu}\\
&+2\|\check{\beta}\|(1+\rho_W)\Pi(\hat{\alpha},q,\dot{q},w,t)\\
&-2\|\check{\beta}\|(1+\rho_W)\Pi(\hat{\alpha},q,\dot{q},w,t)\\
&=2(1+\rho_W)\|\upsilon(\hat{\alpha},q,\dot{q},w,t)\|(1-\frac{\|\upsilon(\hat{\alpha},q,\dot{q},w,t)\|}{\mu})\\
&-2\kappa(1+\rho_W)\underline{\lambda}\|\beta\|^2-2\|\check{\beta}\|(1+\rho_W)(\hat{\alpha}-\alpha)^\top\check{\Pi}(q,\dot{q},w,t)\\
&\le\frac{1}{2}(1+\rho_W)\mu-2\kappa(1+\rho_W)\underline{\lambda}\|\beta\|^2\\
&-2\|\check{\beta}\|(1+\rho_W)(\hat{\alpha}-\alpha)^\top\check{\Pi}(q,\dot{q},w,t).
\end{aligned}\tag{41}$$

Therefore, using (40) and (41), there is

$$\begin{aligned} 2\beta^\top P\dot{\beta} \leq \frac{1}{2}(1+\rho_W)\mu - 2\kappa(1+\rho_W)\underline{\lambda}\|\beta\|^2 \\ - 2\|\breve{\beta}\|(1+\rho_W)(\hat{\alpha}-\alpha)^\top\breve{\Pi}(q,\dot{q},w,t). \end{aligned} \tag{42}$$

for all υ. Subsequently, we will investigate the second term of (31). Based on the adaptive law (24), if $\|\breve{\Pi}\|\|\breve{\beta}\| > \varepsilon$, we have

$$\begin{aligned} &2(1+\rho_W)(\hat{\alpha}-\alpha)^\top\ell_1^{-1}\dot{\hat{\alpha}} \\ &= 2(1+\rho_W)(\hat{\alpha}-\alpha)^\top\breve{\Pi}(q,\dot{q},w,t)\|\breve{\beta}\| \\ &- 2(1+\rho_W)(\hat{\alpha}-\alpha)^\top\ell_1^{-1}\ell_2\hat{\alpha} \\ &\leq 2(1+\rho_W)(\hat{\alpha}-\alpha)^\top\breve{\Pi}(q,\dot{q},t)\|\breve{\beta}\| \\ &- 2(1+\rho_W)\|\hat{\alpha}-\alpha\|^2\ell_1^{-1}\ell_2 + 2(1+\rho_W)\|\hat{\alpha}-\alpha\|\|\alpha\|\ell_1^{-1}\ell_2; \end{aligned} \tag{43}$$

if $\|\breve{\Pi}\|\|\breve{\beta}\| \leq \varepsilon$, we have

$$\begin{aligned} &2(1+\rho_W)(\hat{\alpha}-\alpha)^\top\ell_1^{-1}\dot{\hat{\alpha}} \\ &= 2(1+\rho_W)(\hat{\alpha}-\alpha)^\top\breve{\Pi}(q,\dot{q},w,t)\frac{\|\breve{\Pi}(q,\dot{q},w,t)\|\|\breve{\beta}\|^2}{\varepsilon} \\ &- 2(1+\rho_W)(\hat{\alpha}-\alpha)^\top\ell_1^{-1}\ell_2\hat{\alpha} \\ &\leq 2(1+\rho_W)(\hat{\alpha}-\alpha)^\top\breve{\Pi}(q,\dot{q},t)\|\breve{\beta}\| \\ &- 2(1+\rho_W)\|\hat{\alpha}-\alpha\|^2\ell_1^{-1}\ell_2 + 2(1+\rho_W)\|\hat{\alpha}-\alpha\|\|\alpha\|\ell_1^{-1}\ell_2. \end{aligned} \tag{44}$$

Combining (31), (42) and (43), we can obtain

$$\begin{aligned} \dot{V} \leq \frac{1}{2}(1+\rho_W)\mu - 2\kappa(1+\rho_W)\underline{\lambda}\|\beta\|^2 - 2(1+\rho_W) \\ \times \|\hat{\alpha}-\alpha\|^2\ell_1^{-1}\ell_2 + 2(1+\rho_W)\|\hat{\alpha}-\alpha\|\|\alpha\|\ell_1^{-1}\ell_2. \end{aligned} \tag{45}$$

Combining (31), (42) and (44), we can obtain a result similar to (45) . Let $\varphi(t) := [\beta^\top(q(t),\dot{q}(t),w(t)) \quad (\hat{\alpha}(t)-\alpha)^\top]^\top$, then we have

$$\dot{V} \leq -K_1\|\varphi\|^2 + K_2\|\varphi\| + K_3,$$

where $K_1 = \min\{2\kappa\underline{\lambda}(1+\rho_W), 2(1+\rho_W)\ell_1^{-1}\ell_2\}$, $K_2 = 2(1+\rho_W)\ell_1^{-1}\ell_2\|\alpha\|$, $K_3 = \frac{1}{2}(1+\rho_W)$. Based on the standard arguments on UB and UUB in [22], it can be concluded that $\|\varphi\|$ is uniformly bounded by

$$d(s) = \begin{cases} \sqrt{\frac{\mathcal{X}_2}{\mathcal{X}_1}}R, & \text{if } s \leq R, \\ \sqrt{\frac{\mathcal{X}_2}{\mathcal{X}_1}}s, & \text{if } s > R, \end{cases}$$

$$R = \frac{K_2 + \sqrt{K_2^2 + 4K_1K3}}{2K_1},$$

where $\mathcal{X}_1 = \min\{\lambda_{\min}(P), 2\ell_1^{-1}(1+\rho_W)\}$, $\mathcal{X}_2 = \max\{\lambda_{\max}(P), 2\ell_1^{-1}(1+\rho_W)\}$. Furthermore, $\|\varphi\|$ is uniformly ultimately bounded by

$$\bar{d} = \sqrt{\frac{\mathcal{X}_2}{\mathcal{X}_1}}R,$$

with the time required for $\|\varphi\|$ to converge to the ultimate bound being

$$T(\bar{d}, s) = \begin{cases} 0, & \text{if } s \leq \bar{d}\sqrt{\frac{\mathcal{X}_2}{\mathcal{X}_1}} \\ \frac{\mathcal{X}_2 s^2 - (\mathcal{X}_1^2/\mathcal{X}_2)\bar{d}^2}{K_1\bar{d}^2(\mathcal{X}_1/\mathcal{X}_2) - K_2\bar{d}(\mathcal{X}_1/\mathcal{X}_2)^{1/2} - K_3}, & \text{otherwise.} \end{cases}$$

As a result, both the VFC-following error $\|\beta(q(t),\dot{q}(t),w(t))\|$ and the adaptive error $\|\hat{\alpha}(t)-\alpha\|$ are uniformly bounded and uniformly ultimately bounded (i.e., the trajectory of the uncertain mechanical system (1) approximately follows the constraint defined by (13)). By Proposition 2, we have that the path-following error $\text{dist}(\xi(t), \mathcal{P}^{hgh})$ is uniformly ultimately bounded. Consequently, by Remark 3, the path-following error $\text{dist}(\zeta(t), \mathcal{P})$ is uniformly ultimately bounded. □